
Full-Atom Peptide Design with Geometric Latent Diffusion

Xiangzhe Kong^{1,2} Wenbing Huang^{3,4} Yang Liu^{1,2}

Abstract

Peptide design plays a pivotal role in therapeutics, allowing brand new possibility to leverage target binding sites that are previously undruggable. Most existing methods are either inefficient or only concerned with the target-agnostic design of 1D sequences. In this paper, we propose a generative model for full-atom **Peptide** design with **Geometric LAtent Diffusion** (PepGLAD). We first collect a dataset consisting of both 1D sequences and 3D structures from Protein Data Bank (PDB) and literature, for the training of PepGLAD. We then identify two major challenges of leveraging current diffusion-based models for peptide design: the full-atom geometry and the variable binding geometry. To tackle the first challenge, PepGLAD derives a variational autoencoder that first encodes full-atom residues of variable size into fixed-dimensional latent representations, and then decodes back to the residue space after conducting the diffusion process in the latent space. For the second issue, PepGLAD explores a receptor-specific affine transformation to convert the 3D coordinates into a shared standard space, enabling better generalization ability across different binding shapes. Remarkably, our method improves diversity and *in silico* success rate by 18% and 8% in sequence-structure co-design, and achieves 26% absolute gain in recalling the reference binding conformation.

1. Introduction

Peptides are short chains of amino acids and acts as vital mediators of many protein-protein interactions in human cells. Designing functional peptides has attracted increasing

attention in biological research and therapeutics, since the highly-flexible conformation space of peptides allows brand new possibility to target binding sites that are previously undruggable with antibodies or small molecules (Fosgerau & Hoffmann, 2015; Lee et al., 2019). Diverging from antibody design which inserts Complementarity-Determining Regions (CDRs) into frameworks, and protein design which engineers stable secondary or tertiary structures, peptide design focuses on generating peptides that interact compactly with target proteins (*i.e.*, receptors), since they mostly exhibit flexible conformations (Grathwohl & Wüthrich, 1976) unless bound to receptors (Vanhee et al., 2011). Thus, the key of peptide design lands on capturing the geometry of protein-peptide complexes (see Figure 1).

Conventional simulation or searching algorithms rely on frequent calculations of physical energy functions (Bhardwaj et al., 2016; Cao et al., 2022), which are inefficient and prone to poor local optimum. Recent advances illuminate the remarkable success of exploiting geometric deep generative models, particularly the equivariant diffusion models (Martinkus et al., 2023; Yim et al., 2023), for antibody design (Jin et al., 2021; Luo et al., 2022; Kong et al., 2023) and protein design (Watson et al., 2023; Ingraham et al., 2023). Inspired by these successes, a natural idea of peptide design is leveraging deep generative models as well, which, yet, is challenging in two aspects. From the dataset aspect, there still lacks a peptide dataset consisting of both sequences and structures for the training of deep models. Therefore, this paper first benchmarks the generative models in terms of diversity, consistency, and binding affinity on a dataset that is curated from Protein Data Bank (PDB) (Berman et al., 2000) and the literature (Tsaban et al., 2022). Note that our goal and the constructed dataset here are different from previous works that solely focus on target-agnostic 1D sequences (Muller et al., 2018).

From the methodology aspect, it is nontrivial to adopt diffusion models to characterize the geometry of protein-peptide interactions. The first nontriviality stems from the *full-atom geometry*. The full-atom geometry determines the comprehensive protein-peptide interactions in the atomic level, which is vital yet difficult to preserve. Throughout the generation process, the type of each amino acid always changes and thus requires us to generate different number of atoms, which is unfriendly to diffusion models that prefer fixed-size

*Equal contribution ¹Dept. of Comp. Sci. & Tech., Institute for AI, BNRist Center, Tsinghua University ²Institute for AI Industry Research (AIR), Tsinghua University ³Gaoling School of Artificial Intelligence, Renmin University of China ⁴Beijing Key Laboratory of Big Data Management and Analysis Methods, Beijing, China. Correspondence to: Wenbing Huang <hw@126.com>, Yang Liu <liuyang2011@tsinghua.edu.cn>.

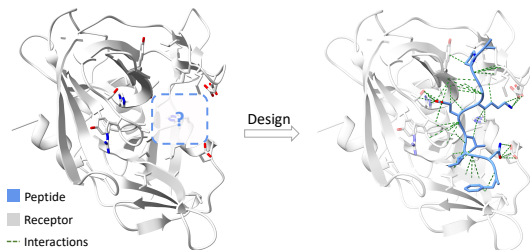


Figure 1. Peptide design requires generating peptides that form compact interactions with the binding site on the receptor. The intricacy of protein-peptide interactions demands efficient exploration in the vast space for sequence-structure co-design.

generation. As a compromise, current models are limited to a constant-size subset of full-atom representations, such as backbone atoms, residue orientations, and side-chain torsional angles (Luo et al., 2022; Watson et al., 2023). The second nontriviality lies in the *variable binding geometry*. Diffusion models are typically implemented directly in the data space, which might be suitable for regular data (e.g. images with fixed value range), yet ill-suited for our case where the rich diversity in the patterns of protein-peptide interactions leads to high variance in the binding geometry in the data space. These variances define divergent target distributions approximating Gaussians with disparate expectations and covariances, which hinders the transferability of diffusions across different binding sites and thereby yields unsatisfactory generalization capability. Unfortunately, this point is seldom investigated in previous diffusion models.

To address the above problems, we propose a powerful model for full-atom **Peptide** design with **Geometric LA**ttent **Diffusion** (PepGLAD). Specifically, we have made the following contributions in this paper:

- To the best of our knowledge, we are the first to exploit deep generative models for end-to-end co-designing both 1D sequences and 3D structures of peptides conditioned on the binding sites. We construct a new training dataset from PDB and literature.
- To capture the *full-atom geometry*, we first learn a Variational AutoEncoder (VAE) to obtain a fixed-size latent representation (including a 3D coordinate and a hidden feature) for each residue of the input peptide, and then conduct the diffusion process in this latent space, both of which are conditional on the binding site to better model protein-peptide interactions. The encoder and the decoder in our VAE are well-designed to enable full-atom input and output, respectively.
- Regarding the *variable binding geometry*, we derive a shared standard space from the binding sites by proposing a novel skill—receptor-specific affine transformation. Such affine transformation is computed by the center offset and covariance Cholesky decomposition

of the binding site coordinates, which actually is the mapping from standard Gaussian to the binding site distribution. Leveraging the inverse of the affine transformation, we are able to convert data space into the standard space and perform generic diffusion therein, which facilitates generalization to diverse binding sites, and even to those unseen shapes during training.

Notably, all the aforementioned models and processes meet the desired symmetry, *i.e.*, $E(3)$ -equivariance, as proved by us. Experiments on sequence-structure co-design and complex conformation generation demonstrate the superiority of our PepGLAD over the existing generative models.

2. Related Work

Peptide Design Conventional methods directly sample residues (Bhardwaj et al., 2016) or building blocks from libraries containing small fragments of proteins (Hossein-zadeh et al., 2021; Swanson et al., 2022; Cao et al., 2022; Bryant & Elofsson, 2022), with guidance from delicate physical energy functions (Alford et al., 2017). These methods are time-consuming and easy to be trapped by local optimum. Recent advances with deep generative models mainly focuses on target-agnostic 1D language models (Muller et al., 2018), antimicrobial peptides (Das et al., 2021; Wang et al., 2022), or a subtype of peptides with α -helix (Xie et al., 2023; Xie12 et al.). While geometric deep generative models are exhibiting notable potential in other domains of target-specific binder design (e.g. small molecules and antibodies), their capability of target-specific peptide design remains unclear due to a lack of benchmark, which is the first problem we tackle in this paper.

Geometric Protein/Antibody Design Protein design primarily aims to generate stable secondary or tertiary structures (Ingraham et al., 2019), where diffusion models demonstrate inspiring performance (Wu et al., 2022; Trippe et al., 2022; Anand & Achim, 2022; Yim et al., 2023). In particular, RFDiffusion (Watson et al., 2023) first generates backbones via diffusion, and then designs the sequences through cycles of inverse folding and structure refining with empirical force fields. Chroma (Ingraham et al., 2023) adopts a similar strategy, but further explores controllable generative process with custom energy functions. Antibody design, encompassing a special family of proteins in the immune system to capture antigens, mainly focuses on in-painting complementarity-determining regions (CDRs) at the interface between the antigen and the framework (Kong et al., 2022; 2023; Verma et al., 2023), where the geometric diffusion models exhibit promising potential (Luo et al., 2022; Martinkus et al., 2023) in co-designing sequence and structure. While peptide design emphasizes the interacting geometry at the interface, it shares similarities with antibody and protein design in that they all consist of linearly con-

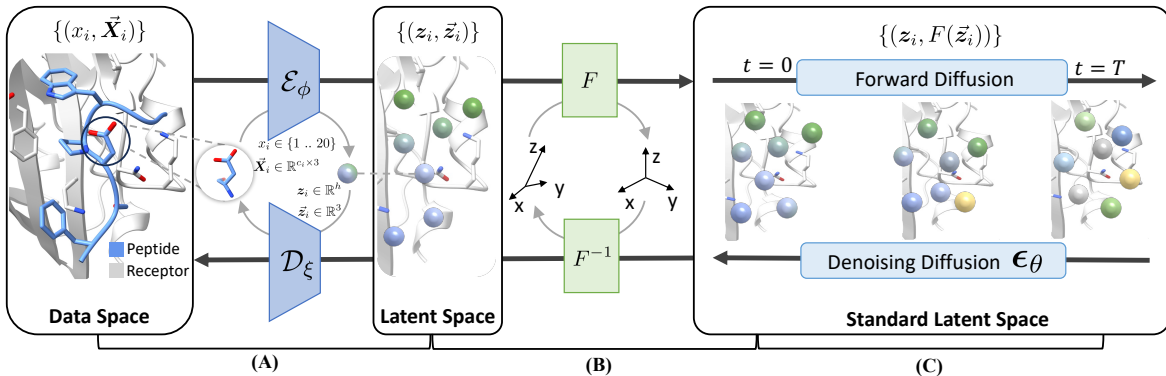


Figure 2. Overall architecture of PepGLAD. (A) Variational AutoEncoder (§3.2): compressing the sequence and the structure $\{(x_i, \vec{X}_i)\}$ of the peptide into the latent space $\{(z_i, \vec{z}_i)\}$ with the encoder \mathcal{E}_ϕ , and decoding the sequence and full-atom geometry from the latent states with the decoder \mathcal{D}_ξ . (B) Affine Transformation F (§3.3): projecting the geometry to approximately $\mathcal{N}(\mathbf{0}, \mathbf{I})$ via the receptor-specific affine transformation derived from the binding site, and recovering the data geometry with the inverse of F after the diffusion generative process. (C) Latent Diffusion (§3.4): jointly generating z_i and \vec{z}_i in the standard latent space.

nected amino acids. Therefore, we initially explore models from these two domains in the context of peptide design.

Equivariant Diffusion Models Diffusion models learn a denoising trajectory to generate desired data distribution from a prior distribution, commonly standard Gaussian (Sohl-Dickstein et al., 2015; Song & Ermon, 2019; Ho et al., 2020). Recent literature extends diffusion to 3D small molecules satisfying the E(3)-equivariance (Xu et al., 2022), which triggers subsequent advances in geometric design of macro molecules (*e.g.* antibody, protein) as aforementioned. In this paper, we further explore a diffusion process that still preserves the equivariance under data-specific affine transformations. Moreover, our work is closely related to latent diffusion models, which implement the generative process in the compressed latent space encoded by pretrained autoencoders (Rombach et al., 2022; Xu et al., 2023).

3. Our Method: PepGLAD

We first define the notations in the paper and formalize peptide design in §3.1. The overall workflow of our PepGLAD is presented in Figure 2, which consists of three modules: (1) An autoencoder that defines the joint latent space for sequences and structures conditioned on the full-atom context of the binding site (§3.2); (2) An affine transformation derived from the binding site to project the 3D geometry into a standard space approximating standard Gaussian distribution (§3.3); (3) A latent diffusion model trained on the standard latent space (§3.4). Finally, we summarize the training and the sampling procedures in §3.5.

3.1. Definitions and Notations

We represent binding sites and peptides as geometric graphs $\mathcal{G} = \{(x_i, \vec{X}_i)\}$, where each node i is a residue with its amino acid type x_i and the coordinates of all its c_i atoms

$\vec{X}_i \in \mathbb{R}^{c_i \times 3}$. In later sections, we use the simplified notations $i \in \mathcal{G}$ to denote that a node i is in the geometric graph \mathcal{G} , and $|\mathcal{G}|$ to denote the total number of nodes in \mathcal{G} . We use \mathcal{G}_p and \mathcal{G}_b to represent the geometric graph of the peptide and the binding site, respectively.

Task Definition Given the binding site \mathcal{G}_b , we aim to obtain a generative model p_θ conforming to the distribution of binding peptides $q(\mathcal{G}_p|\mathcal{G}_b)$.

3.2. Variational AutoEncoder

The autoencoder (Vincent et al., 2010) consists of an encoder \mathcal{E}_ϕ that encodes the peptide \mathcal{G}_p in the presence of the binding site \mathcal{G}_b into a latent state \mathcal{G}_z , and a decoder \mathcal{D}_ξ that reconstructs the peptide from the latent state to obtain $\mathcal{G}'_p = \{(x'_i, \vec{X}'_i)\}$. To encourage \mathcal{E}_ϕ to learn contextual representations of residues, we corrupt 25% of the residues in \mathcal{G}_p with a [MASK] type to obtain $\tilde{\mathcal{G}}_p$ as the input:

$$\mathcal{G}_z = \mathcal{E}_\phi(\tilde{\mathcal{G}}_p, \mathcal{G}_b), \quad (1)$$

$$\mathcal{G}'_p = \mathcal{D}_\xi(\mathcal{G}_z, \mathcal{G}_b), \quad (2)$$

where $\mathcal{G}_z = \{(z_i, \vec{z}_i) | i \in \mathcal{G}_p\}$ contains the latent states $z_i \in \mathbb{R}^h$ ($h = 8$ in this paper) and $\vec{z}_i \in \mathbb{R}^3$ sampled from the encoded distribution $\mathcal{N}(z_i; \mu_i, \sigma_i)$ and $\mathcal{N}(\vec{z}_i; \vec{\mu}_i, \vec{\sigma}_i)$ using the reparameterization trick (Kingma & Welling, 2013). We borrow the adaptive multi-channel equivariant encoder in dyMEAN (Kong et al., 2023) for both \mathcal{E}_ϕ and \mathcal{D}_ξ to capture the full-atom geometry. In the decoder \mathcal{D}_ξ , we factorize the joint distribution of sequences and structures as follows:

$$p_\xi(x'_i, \vec{X}'_i | \mathcal{G}_z, \mathcal{G}_b) = p_{\xi_1}(x'_i | \mathcal{G}_z, \mathcal{G}_b) p_{\xi_2}(\vec{X}'_i | x'_i, \mathcal{G}_z, \mathcal{G}_b), \quad (3)$$

where the sequence is first decoded and then the all-atom geometry, initialized with replications of \vec{z}_i , is reconstructed. The training objective of the autoencoder consists of the reconstruction loss \mathcal{L}_{recon} and the KL divergence \mathcal{L}_{KL} to

constrain the latent space. The reconstruction loss includes cross entropy on the residue types, mean square error (MSE) on the full-atom structures, and an auxiliary loss \mathcal{L}_{aux} on bond lengths and angles (Jumper et al., 2021):

$$\mathcal{L}_{recon}(i) = H(p(x_i), p(x'_i)) + \text{MSE}(\vec{X}_i, \vec{X}'_i) + \mathcal{L}_{aux}(i), \quad (4)$$

where H denotes cross entropy. We include details of \mathcal{L}_{aux} in Appendix A. The KL divergence constrains z_i and \vec{z}_i with the prior $\mathcal{N}(\mathbf{0}, \mathbf{I})$ and $\mathcal{N}(\vec{r}_i, \mathbf{I})$, respectively, where \vec{r}_i denotes the coordinate of the alpha carbon (C_α) in node i :

$$\mathcal{L}_{KL}(i) = \lambda_1 \cdot D_{KL}(\mathcal{N}(\mathbf{0}, \mathbf{I}) \| \mathcal{N}(\mu_i, \text{diag}(\sigma_i))) + \lambda_2 \cdot D_{KL}(\mathcal{N}(\vec{r}_i, \mathbf{I}) \| \mathcal{N}(\vec{\mu}_i, \text{diag}(\vec{\sigma}_i))), \quad (5)$$

where D_{KL} denotes the KL divergence, λ_1 and λ_2 reweight the constraints on the sequence and the structure, respectively. \mathcal{L}_{KL} prevents the scale of z_i from exploding and constrains \vec{z}_i around C_α to retain necessary geometric information. Then we have the overall training objective of the variational autoencoder as follows:

$$\mathcal{L}_{AE} = \sum_{i \in \mathcal{G}_p} (\mathcal{L}_{recon}(i) + \mathcal{L}_{KL}(i)) / |\mathcal{G}_p|. \quad (6)$$

3.3. Receptor-Specific Affine Transformation

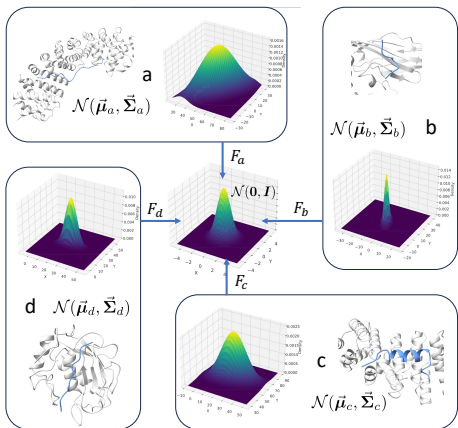


Figure 3. Different binding sites (a, b, c, d) adopt disparate center offsets and geometric shapes, approximating variable 3D Gaussian distributions that deviate from $\mathcal{N}(\mathbf{0}, \mathbf{I})$. We propose to convert the geometry into a standard space approximating standard Gaussian, via an affine transformation derived from the binding site (§3.3).

With the latent space given by the autoencoder, we further exploit a standard space obtained from receptor-specific affine transformations, which enhances the transferability of diffusions on disparate binding sites (see Figure 3). Most peptides fold into complementary shape upon binding on the receptor (Vanhee et al., 2011; London et al., 2010). Thus, the target distribution is inherently characterized by the shape of the binding site. Given the wide disparity in binding geometries, directly implementing diffusion in the data space

yields minimal transferability among different binding sites. To address this deficiency, we propose to implement the diffusion process on a shared standard space converted via an affine transformation derived from the binding site. Formally, denoting the C_α coordinates of the residues in a given binding site \mathcal{G}_b as $\vec{R} \in \mathbb{R}^{3 \times |\mathcal{G}_b|}$, we can derive their center $\vec{\mu} \in \mathbb{R}^3$ and covariance $\vec{\Sigma} \in \mathbb{R}^{3 \times 3}$:

$$\vec{\mu} = \mathbb{E}[\vec{R}], \vec{\Sigma} = \text{Cov}(\vec{R}, \vec{R}), \quad (7)$$

so that these coordinates can be regarded as sampled from the distribution $\mathcal{N}(\vec{\mu}, \vec{\Sigma})$. We then calculate the Cholesky decomposition (Golub & Van Loan, 2013) of $\vec{\Sigma}$:

$$\vec{\Sigma} = \vec{L}\vec{L}^\top, \vec{L} \in \mathbb{R}^{3 \times 3}, \quad (8)$$

where \vec{L} is a lower triangular matrix. \vec{L} is unique (Golub & Van Loan, 2013) and invertible since the covariance matrix is a real-valued symmetric positive-definite matrix¹. Then we can define the affine transformation $F : \mathbb{R}^3 \rightarrow \mathbb{R}^3$:

$$F(\vec{x}) = \vec{L}^{-1}(\vec{x} - \vec{\mu}), \quad (9)$$

which enables the projection of the geometry into the standard space approximating standard Gaussian $F(\vec{R}) \sim \mathcal{N}(\mathbf{0}, \mathbf{I})$. Further, we can easily obtain the inverse of F_b as:

$$F^{-1}(\vec{x}) = \vec{L}\vec{x} + \vec{\mu}. \quad (10)$$

With the above definitions, for each given binding site \mathcal{G}_b , we transform the geometry via the derived F to obtain the standard space, where the diffusion model is implemented, and recover the original geometry with F^{-1} (see Figure 2) after generation. Notably, we have the following proposition to ensure that the equivariance is maintained under the proposed affine transformation with scalarization-based equivariant GNNs (Han et al., 2022; Duval et al., 2023):

Proposition 3.1. *Denote the invariant and equivariant outputs from a scalarization-based $E(3)$ -equivariant GNN as $f(\{\mathbf{h}_i, \vec{x}_i\})$ and $\vec{f}(\{\mathbf{h}_i, \vec{x}_i\})$, respectively. With the definition of F in Eq. 9, $\forall g \in E(3)$, we have $f(\{\mathbf{h}_i, F(\vec{x}_i)\}) = f(\{\mathbf{h}_i, F_g(g \cdot \vec{x}_i)\})$ and $g \cdot F^{-1}(\vec{f}(\{\mathbf{h}_i, F(\vec{x}_i)\})) = F_g^{-1}(\vec{f}(\{\mathbf{h}_i, F_g(g \cdot \vec{x}_i)\}))$, where F_g is derived on the coordinates transformed by g . Namely, the $E(3)$ -equivariance is preserved if we implement the GNN on the standard space and recover the original geometry from the outputs.*

We provide the proof in Appendix B. This is vital since it indicates the Markov kernel is $E(3)$ -equivariant, and thus ensures the $E(3)$ -invariance of the probability density in the diffusion process (Xu et al., 2022).

¹The binding site has at least 3 nonoverlapping nodes, namely $\text{rank}(\vec{R}) = 3$, thus we can ignore the corner case of semi-positive definite matrices.

3.4. Geometric Latent Diffusion Model

With the aforementioned preparations, the discrete residue types are encoded as continuous latent representations $\{z_i\}$, and the full-atom geometry is also compressed and standardized into 3D vectors $\{\bar{z}_i\} \sim \mathcal{N}(\mathbf{0}, \mathbf{I})$. Therefore, we are ready to implement a diffusion model on the standard latent space to generate z_i and \bar{z}_i . The forward diffusion process gradually adds noise to the data from $t = 0$ to $t = T$, resulting in the prior distribution $\mathcal{N}(\mathbf{0}, \mathbf{I})$. The reverse diffusion process generates data distribution by iteratively denoising the distribution from $t = T$ to $t = 0$. We denote $\bar{\mathbf{u}}_i^t = [z_i^t, \bar{z}_i^t]$ and $\mathcal{G}_z^t = \{(z_i^t, \bar{z}_i^t)\}$ as the intermediate state for node i and the entire peptide at time step t , respectively. For simplicity, we assume both \mathcal{G}_z^t and the binding site \mathcal{G}_b are already standardized via the transformation F_b in Eq. 9. Then we have the forward process as:

$$q(\bar{\mathbf{u}}_i^t | \bar{\mathbf{u}}_i^{t-1}) = \mathcal{N}(\bar{\mathbf{u}}_i^t; \sqrt{1 - \beta^t} \cdot \bar{\mathbf{u}}_i^{t-1}, \beta^t \mathbf{I}), \quad (11)$$

$$q(\bar{\mathbf{u}}_i^t | \bar{\mathbf{u}}_i^0) = \mathcal{N}(\bar{\mathbf{u}}_i^t; \sqrt{\bar{\alpha}^t} \cdot \bar{\mathbf{u}}_i^0, (1 - \bar{\alpha}^t) \mathbf{I}), \quad (12)$$

where β^t is the noise scale increasing with the timestep from 0 to 1 conforming to the cosine schedule (Nichol & Dhariwal, 2021), and $\bar{\alpha}^t = \prod_{s=1}^{s=t} (1 - \beta^s)$. Then the state at timestep t can be sampled as:

$$\bar{\mathbf{u}}_i^t = \sqrt{\bar{\alpha}^t} \bar{\mathbf{u}}_i^0 + (1 - \bar{\alpha}^t) \epsilon_i, \quad (13)$$

where $\epsilon_i \sim \mathcal{N}(\mathbf{0}, \mathbf{I})$. Following Ho et al. (2020), the reverse process can be defined with the reparameterization trick as:

$$p_\theta(\bar{\mathbf{u}}_i^{t-1} | \mathcal{G}_z^t, \mathcal{G}_b) = \mathcal{N}(\bar{\mathbf{u}}_i^{t-1}; \bar{\boldsymbol{\mu}}_\theta(\mathcal{G}_z^t, \mathcal{G}_b), \beta^t \mathbf{I}), \quad (14)$$

$$\bar{\boldsymbol{\mu}}_\theta(\mathcal{G}_z^t, \mathcal{G}_b) = \frac{1}{\sqrt{\bar{\alpha}^t}} (\bar{\mathbf{u}}_i^t - \frac{\beta^t}{\sqrt{1 - \bar{\alpha}^t}} \epsilon_\theta(\mathcal{G}_z^t, \mathcal{G}_b, t)[i]), \quad (15)$$

where $\alpha^t = 1 - \beta^t$, and ϵ_θ is the denoising network also implemented with the equivariant adaptive multi-channel equivariant encoder in dyMEAN (Kong et al., 2023) to retain full-atom context of the binding site during generation and preserve the equivariance under affine transformations (Proposition 3.1). Finally, we have the objective at time step t as MSE between the predicted noise and the added noise in Eq. 13, as well as the overall training objective \mathcal{L}_{LDM} as the expectation with respect to t :

$$\mathcal{L}_{LDM}^t = \sum_i \|\epsilon_i - \epsilon_\theta(\mathcal{G}_z^t, \mathcal{G}_b, t)[i]\|^2 / |\mathcal{G}_z^t|, \quad (16)$$

$$\mathcal{L}_{LDM} = \mathbb{E}_{t \sim \text{Uniform}(1..T)} [\mathcal{L}_{LDM}^t] \quad (17)$$

3.5. Training and Sampling

Training The training of our PepGLAD can be divided into two phases where a variational autoencoder is first trained and then a diffusion model is trained on the standard latent space. We provide the overall training procedure in Algorithm 1. Note that a smooth and informative latent space is

necessary for the consecutive training of the diffusion model, thus we resort to unsupervised data from protein fragments apart from the limited protein-peptide complexes for training the autoencoder, which we describe in Appendix D.

Algorithm 1 Training Algorithm of PepGLAD

input geometric data of protein-peptide complexes \mathcal{S}
output encoder \mathcal{E}_ϕ , decoder \mathcal{D}_ξ , denoising network ϵ_θ

- 1: **function** TrainAutoEncoder(\mathcal{S})
- 2: Initialize $\mathcal{E}_\phi, \mathcal{D}_\xi$
- 3: **while** ϕ, ξ have not converged **do**
- 4: Sample $(\mathcal{G}_p, \mathcal{G}_b) \sim \mathcal{S}$
- 5: $\tilde{\mathcal{G}}_p \leftarrow \text{mask}(\mathcal{G}_p)$ {Mask 25% Residues}
- 6: $\{(\boldsymbol{\mu}_i, \boldsymbol{\sigma}_i, \bar{\boldsymbol{\mu}}_i, \bar{\boldsymbol{\sigma}}_i)\} \leftarrow \mathcal{E}_\phi(\tilde{\mathcal{G}}_p, \mathcal{G}_b)$ {Encoding}
- 7: $\{(\boldsymbol{\epsilon}_i, \bar{\boldsymbol{\epsilon}}_i)\} \sim \mathcal{N}(\mathbf{0}, \mathbf{I})$ {Reparameterization}
- 8: $\mathcal{G}_z \leftarrow \{(\boldsymbol{\mu}_i + \boldsymbol{\epsilon}_i \odot \boldsymbol{\sigma}_i, \bar{\boldsymbol{\mu}}_i + \bar{\boldsymbol{\epsilon}}_i \odot \bar{\boldsymbol{\sigma}}_i)\}$
- 9: $\mathcal{G}'_p \leftarrow \mathcal{D}_\xi(\mathcal{G}_z, \mathcal{G}_b)$ {Decoding}
- 10: $\mathcal{L}_{AE} = \sum_{i \in \mathcal{G}'_p} (\mathcal{L}_{recon}(i) + \mathcal{L}_{KL}(i)) / |\mathcal{G}'_p|$
- 11: $\phi, \xi \leftarrow \text{optimizer}(\mathcal{L}_{AE}; \phi, \xi)$
- 12: **end while**
- 13: **return** $\mathcal{E}_\phi, \mathcal{D}_\xi$
- 14: **end function**
- 15:
- 16: **function** TrainLatentDiffusion($\mathcal{E}_\phi, \mathcal{D}_\xi, \mathcal{S}$)
- 17: Initialize ϵ_θ
- 18: **while** θ have not converged **do**
- 19: Sample $(\mathcal{G}_p, \mathcal{G}_b) \sim \mathcal{S}$
- 20: $\{(\boldsymbol{\mu}_i, \boldsymbol{\sigma}_i, \bar{\boldsymbol{\mu}}_i, \bar{\boldsymbol{\sigma}}_i)\} \leftarrow \mathcal{E}_\phi(\mathcal{G}_p, \mathcal{G}_b)$ {Encoding}
- 21: $\mathcal{G}_z^0 \leftarrow \{(\boldsymbol{\mu}_i, \bar{\boldsymbol{\mu}}_i)\}$
- 22: $F \leftarrow \text{affine}(\mathcal{G}_b)$ {Affine Transformation}
- 23: $\mathcal{G}_z^0, \mathcal{G}_b \leftarrow F(\mathcal{G}_z^0), F(\mathcal{G}_b)$ {Standard Geometry}
- 24: $\{(\mathbf{z}_i^0, \bar{\mathbf{z}}_i^0)\} \leftarrow \mathcal{G}_z^0$
- 25: $t \sim \mathbf{U}(1, T)$, $\{(\boldsymbol{\epsilon}_i, \bar{\boldsymbol{\epsilon}}_i)\} \sim \mathcal{N}(\mathbf{0}, \mathbf{I})$
- 26: $\mathcal{G}_z^t \leftarrow \{\sqrt{\bar{\alpha}^t}[\mathbf{z}_i^0, \bar{\mathbf{z}}_i^0] + (1 - \bar{\alpha}^t)[\boldsymbol{\epsilon}_i, \bar{\boldsymbol{\epsilon}}_i]\}$
- 27: $\mathcal{L}_{LDM}^t = \sum_i \|\boldsymbol{\epsilon}_i, \bar{\boldsymbol{\epsilon}}_i - \epsilon_\theta(\mathcal{G}_z^t, \mathcal{G}_b, t)[i]\|^2 / |\mathcal{G}_z^t|$
- 28: $\theta \leftarrow \text{optimizer}(\mathcal{L}_{LDM}^t; \theta)$
- 29: **end while**
- 30: **return** ϵ_θ
- 31: **end function**
- 32:
- 33: $\mathcal{E}_\phi, \mathcal{D}_\xi \leftarrow \text{TrainAutoEncoder}(\mathcal{S})$
- 34: Fix parameters ϕ and ξ
- 35: $\epsilon_\theta \leftarrow \text{TrainLatentDiffusion}(\mathcal{E}_\phi, \mathcal{D}_\xi, \mathcal{S})$
- 36: **return** $\mathcal{E}_\phi, \mathcal{D}_\xi, \epsilon_\theta$

Sampling in Ordered Subspace The sampling procedure includes generative diffusion process on the standard latent states, recovering the original geometry with the inverse of F in Eq. 9, and decoding the sequence as well as the full-atom structure of the peptide (see Algorithm 2). A problem here is that the unordered nature of graphs is not compatible with the sequential nature of peptides, thus the generated residues may have arbitrary permutation on the sequence order. Inspired by the concept of classifier-guided

sampling (Dhariwal & Nichol, 2021), we first assign an arbitrary permutation \mathcal{P} on the sequence order to the nodes. Then we steer the sampling procedure towards the desired subspace conforming to \mathcal{P} with the following empirical classifier $p(1|\{\mathbf{z}_i^t\})$, which estimates the probability of the current coordinates belonging to the desired subspace:

$$p(1|\{\mathbf{z}_i^t\}) = \exp(-\sum_{\mathcal{P}(i)-\mathcal{P}(j)=1} E(\|\mathbf{z}_i^t - \mathbf{z}_j^t\|)), \quad (18)$$

$$E(d) = \begin{cases} d - (\mu_d + 3\sigma_d), & d > \mu_d + 3\sigma_d, \\ (\mu_d - 3\sigma_d) - d, & d < \mu_d - 3\sigma_d, \\ 0, & \text{otherwise,} \end{cases} \quad (19)$$

where μ_d and σ_d are the mean and variance of the distances of adjacent residues in the latent space measured from the training set. Intuitively, this classifier gives higher confidence if the adjacent (defined by \mathcal{P}) residues are within reasonable distances aligning with the statistics from the training set. We provide more details in Appendix E.

Algorithm 2 Sampling Algorithm of PepGLAD

```

input decoder  $\mathcal{D}_\xi$ , denoising network  $\epsilon_\theta$ , binding site  $\mathcal{G}_b$ 
output peptide  $\mathcal{G}_p$ 
1:  $F \leftarrow \text{affine}(\mathcal{G}_b)$            {Affine Transformation}
2:  $\mathcal{G}_b \leftarrow F(\mathcal{G}_b)$          {Standard Geometry}
3:  $\{(\mathbf{z}_i^T, \bar{\mathbf{z}}_i^T)\} \sim \mathcal{N}(\mathbf{0}, \mathbf{I})$ 
4: for  $t$  in  $T, T-1, \dots, 1$  do
5:    $\mathcal{G}_z^t \leftarrow \{(\mathbf{z}_i^t, \bar{\mathbf{z}}_i^t)\}$    {Latent Denoising Loop}
6:    $\bar{\mathbf{u}}_i^t \leftarrow \mathbf{z}_i^t, \bar{\mathbf{z}}_i^t$ 
7:    $\epsilon_i = [\epsilon_i, \bar{\epsilon}_i] \sim \mathcal{N}(\mathbf{0}, \mathbf{I})$ 
8:    $\bar{\mathbf{u}}_i^{t-1} \leftarrow \frac{1}{\sqrt{\alpha^t}}(\bar{\mathbf{u}}_i^t - \frac{\beta^t}{\sqrt{1-\alpha^t}}\epsilon_\theta(\mathcal{G}_z^t, \mathcal{G}_b, t)[i]) + \beta_t \epsilon_i$ 
9:    $[\mathbf{z}_i^{t-1}, \bar{\mathbf{z}}_i^{t-1}] \leftarrow \bar{\mathbf{u}}_i^{t-1}$ 
10: end for
11:  $\mathcal{G}_z \leftarrow \{(\mathbf{z}_i^0, \bar{\mathbf{z}}_i^0)\}$ 
12:  $\mathcal{G}_z, \mathcal{G}_b \leftarrow F^{-1}(\mathcal{G}_z), F^{-1}(\mathcal{G}_b)$    {Data Geometry}
13:  $\mathcal{G}_p \leftarrow \mathcal{D}_\xi(\mathcal{G}_z, \mathcal{G}_b)$            {Decoding}
14: return  $\mathcal{G}_p$ 

```

4. Experiments

4.1. Setup

Task We evaluate our PepGLAD and baselines on the following tasks: (1) **sequence-structure co-design** (§4.2) aims to generate both the sequence and the structure of the peptide given the specific binding site on the receptor (*i.e.* protein). (2) **Binding Conformation Generation** (§4.3) requires to generate the binding state of the peptide given its sequence and the binding site of interest.

Dataset We first extract all dimers from the Protein Data Bank (PDB) (Berman et al., 2000) and filter out the complexes with a receptor longer than 30 residues and a ligand between 4 to 25 residues (Tsaban et al., 2022). Then we remove the duplicated complexes with the criterion that both the receptor and the peptide has a sequence identity

over 90% (Steinegger & Söding, 2017), after which 6105 non-redundant complexes are obtained. To achieve the cross-target generalization test, we utilize the large non-redundant dataset (LNR) from Tsaban et al. (2022) as the test set, which contains 93 protein-peptide complexes with canonical amino acids curated by domain experts. We then cluster the data by receptor with a sequence identity threshold of over 40%, and remove the complexes sharing the same clusters with those from the test set. Finally, the remaining data are randomly split based on clustering results into training and validation sets. Further, we exploit 70k unsupervised data from protein fragments (ProtFrag) to facilitate training of the variational autoencoder. Table 1 provides statistics on these datasets, with further details in Appendix D.

Table 1. Statistics of the constructed datasets.

Split	#entry	#cluster	source
Training	4,157	952	PDB (Berman et al., 2000)
Validation	114	50	PDB (Berman et al., 2000)
Test	93	93	LNR (Tsaban et al., 2022)
ProtFrag	70,645	-	monomers in PDB

Baselines We first borrow three baselines from the antibody design domain. **HSRN** (Jin et al., 2022) autoregressively decodes the sequence while keeps refining the structure hierarchically, from the C_α to other atoms. **dyMEAN** (Kong et al., 2023) is equipped with an full-atom geometric encoder and exploits iterative non-autoregressive generation. **DiffAb** (Luo et al., 2022) jointly diffuses on the categorical residue type, the coordinate of C_α as well as the orientation of each residue. Next, we explore two baselines from the general protein design. **RFDiffusion** (Watson et al., 2023) exploits a pipeline that first generates the backbone via diffusion and then alternates between inverse folding (Dauparas et al., 2022) and structure refining based on a physical energy function (Alford et al., 2017). **AlphaFold 2** (Jumper et al., 2021) is the well-known model for protein folding, which also shows certain abilities on peptide conformation prediction (Tsaban et al., 2022). We also include two traditional methods. **AnchorExtension** (Hosseinzadeh et al., 2021) designs peptides by first docking an existing scaffold to the binding site, and then optimizing the peptide with cycles of mutations guided by energy functions. **FlexPep-Dock** (London et al., 2011) is designed for flexible peptide docking via optimization in the landscape of a physical energy function (Alford et al., 2017). Implementation details are provided in Appendix G.

4.2. Sequence-Structure Co-Design

Metrics A favorable generative model should produce diverse candidates while maintaining fidelity to the desired distribution. To assess the generative performance and generalization ability, we generate 40 candidates for each receptor and employ the following metrics:

- **Diversity.** Inspired (Yim et al., 2023), we measure the diversity of candidates via unique clusters of sequences and structures. Specifically, we hierarchically cluster the structures based on pair-wise root mean square deviation (RMSD) of C_{α} . The diversity of structures Div_{struct} is defined as the number of clusters versus the number of candidates. A similar procedure can be applied to the sequences, utilizing the similarity (Lei et al., 2021) derived from alignment using BLOSUM62 matrix (Henikoff & Henikoff, 1992), to obtain the diversity of sequences Div_{seq} . Then we calculate the co-design diversity as $\sqrt{Div_{seq}Div_{struct}}$.
- **Consistency.** We measure how well the models learn the 1D&3D joint distribution by the consistency between the generated sequences and structures, quantified via Cramér’s V (Cramér, 1999) association between the clustering labels (as in Diversity) of the sequences and the structures. High consistency indicates that candidates with similar sequences also have similar structures, implying that the generative model effectively captures the dependency between 1D and 3D.
- **ΔG .** Aligned with the literature (Kong et al., 2023; Luo et al., 2022), we employ the binding energy (kcal/mol) provided by Rosetta (Alford et al., 2017), a widely-used suite for biomolecular modeling using physical energy functions, to evaluate the binding affinity of the generated candidates. Lower ΔG indicates stronger binding between the peptide and the target.
- **Success.** We report the proportion of successful designs (*i.e.* $\Delta G < 0$) among all the candidates.

For all metrics except ΔG , we first compute values for each receptor individually and then average the results across different receptors. For ΔG , we identify the best candidate on each receptor as the outputs and report the median value across different receptors. Details on implementation and discussion of the metrics are provided in Appendix F.

Table 2. Evaluation on sequence-structure co-design. On each target, 40 candidates are generated for evaluation. Div. and Con. are abbreviations for diversity and consistency, respectively.

Model	Div.(↑)	Con.(↑)	ΔG (↓)	Success
Test Set	-	-	-35.25	95.70%
HSRN ²	0.158	0.0	≥ 0	10.46%
dyMEAN	0.150	0.0	-2.26	14.60%
DiffAb	0.427	0.670	-21.20	49.87%
PepGLAD (ours)	0.506	0.789	-21.94	55.97%

Results Table 2 illustrates that our PepGLAD generates significantly more diversified and consistent peptides with better binding energy and success rates compared to the baselines. When benchmarking HSRN, dyMEAN, and DiffAb,

²HSRN and dyMEAN generate homogeneous structures that are clustered together yet still sample very different sequences, leading to zero association between sequence and structure.

which perform well on antibody CDR design, we observe a notable performance gap between non-diffusion baselines (*i.e.* HSRN, dyMEAN) and the diffusion-based baseline (*i.e.* DiffAb), suggesting the higher complexity in peptide design and the need for stronger modeling capabilities. Compared to DiffAb, which operates on categorical residue types, backbone coordinates and residue orientations, our PepGLAD (1) better captures the dependency between sequence and structure, as indicated by higher diversity and consistency, since diffusion is implemented on the latent space where the representation of sequence and structure are nicely correlated by the autoencoder; (2) more effectively captures the intricate protein-peptide interactions, demonstrated by better ΔG and success rates, since we leverage the full-atom context of the binding site and enhances generalization capability by converting the geometry into a standard space. We showcase two candidates designed by our PepGLAD with favorable binding energy (ΔG) given by Rosetta in Figure 4.

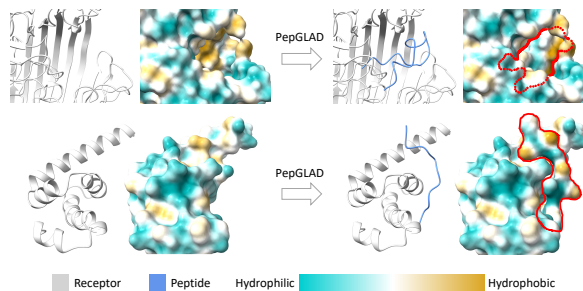


Figure 4. **Top:** A generated candidate confined within the binding site (PDB=4cu4, $\Delta G=-34.21$). **Bottom:** A generated candidate with complementary shape to the binding site (PDB=3pkn, $\Delta G=-33.32$). Both candidates form compact interactions at the interface.

We also evaluate our PepGLAD against two sophisticated pipeline systems in Table 3. The traditional method (*i.e.* AnchorExtension) is limited by low efficiency, thus we can only afford outputting 10 candidates for each receptor. For a relatively fair comparison with RFDiffusion, we refine the structure of the generated candidates using the empirical force field in RFDiffusion once. However, the comparison may still disadvantage our PepGLAD, given that RFDiffusion is finetuned from a model pretrained on a large-scale dataset (Watson et al., 2023). As demonstrated in Table 3, our model still exhibits marvelous superiority on diversity, consistency, and success rate, while achieving competitive binding energy ΔG , with obviously higher efficiency.

Table 3. Evaluation on sequence-structure co-design with two well-established systems. Time cost is measured as the total time spent divided by the number of designed candidates.

Model	Div.(↑)	Con.(↑)	ΔG (↓)	Success	Time
AnchorExtension	0.245	0.423	-26.80	84.30%	735s
RFDiffusion	0.259	0.696	-33.82	79.68%	61s
PepGLAD (ours)	0.506	0.789	-29.36	92.82%	3s

4.3. Binding Conformation Generation

Metrics For each receptor, we generate 10 candidates and calculate the following metrics:

- **RMSD_{C α}** . Root mean square deviation on the coordinates of C α between a candidate and a reference structure with the unit Å. RMSD values below 5Å and 2Å typically indicate near-native and high-quality conformations, respectively (Weng et al., 2020).
- **DockQ** (Basu & Wallner, 2016). A comprehensive metric evaluating the full-atom similarity on the interface between a candidate and a reference complex. It ranges from 0 to 1, with values above 0.49 and 0.80 considered as medium and high quality, respectively.

To measure how well the generated distribution can recover the reference conformation, we first identify the candidate with the best score on each receptor as the final output, then report the median score and the proportion of the outputs satisfying certain thresholds across different receptors.

Table 4. Evaluation on binding conformation generation. On each target, 10 candidates are generated to calculate the best recall of the reference conformation.

Model	RMSD _{Cα} (↓)			DockQ(↑)		
	%≤ 2	%≤ 5	median	%≥ .80	%≥ .49	median
FlexPepDock	0.0	25.0	6.43	0.0	28.3	0.393
dyMEAN	0.0	12.9	7.96	0.0	29.0	0.374
HSRN	0.0	31.2	6.02	3.2	53.8	0.508
AlphaFold 2	14.0	36.6	8.49	18.3	43.0	0.355
DiffAb	11.8	60.2	4.23	21.5	67.7	0.586
PepGLAD (ours)	19.4	86.0	3.16	24.7	88.2	0.675

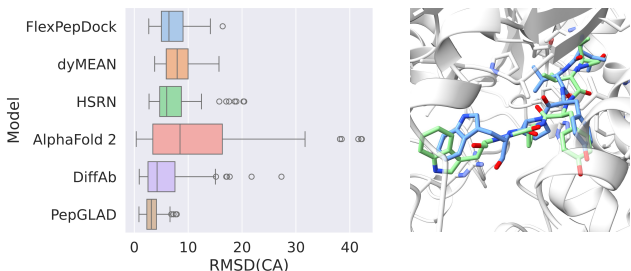


Figure 5. **Left:** The distribution of RMSD_{C α} on the test set from different models. **Right** (PDB=3t6j): A candidate conformation (blue) generated by our PepGLAD with RMSD_{C α} = 1.35Å and DockQ= 0.93 to the reference (blue).

Results As shown in Table 4, our PepGLAD surpasses all the baselines in terms of both RMSD_{C α} and DockQ by a large margin, highlighting the superiority of incorporating the full-atom context and the binding-site shape into the latent diffusion process. Additionally, we present the distribution of the best RMSD_{C α} on different test receptors using box plots and showcase a generated conformation highly resembling the reference in Figure 5. The distribution reveals that our model achieves favorable performance on RMSD_{C α} with lower variance on the test set compared to other baselines, exhibiting robust generalization ability across disparate binding sites.

5. Analysis

We conduct ablations on the following components to verify their necessity: the full-atom geometry (**Full-Atom**); the affine transformation to convert the geometry into the standard space (**Affine**); the unsupervised data from protein fragments (**ProtFrag**) and the mask policy (**Mask**) when training the variational autoencoder. Note that generative performance is assessed from various aspects, and improvement in one aspect at the disproportionate expense of others might be meaningless. Thus, we additionally compute the average of all the metrics to evaluate the comprehensive effect of each module, where ΔG is normalized by the statistics on the test set. Table 5 demonstrates the following observations: (1) Discarding the full-atom context results in a significant degradation on all metrics, especially the success rate, implying the necessity of the full-atom context in capturing the intricate protein-peptide interactions; (2) Implementing the diffusion directly on the data space without the proposed affine transformation incurs a notably adverse impact on all metrics, indicating the remarkable enhancement on the generalization capability made by the affine transformation; (3) Training without the unsupervised data leads to a less informative latent space, exerting a negative effect on the binding energy and success rate; (4) Removal of the mask policy reduces the correlation between sequence and structure in the latent space, thus harms the consistency.

Table 5. Ablations on different components. Avg. computes the average of all metrics, where ΔG is first normalized by the median value of the references on test set.

Ablations	Div.(↑)	Con.(↑)	ΔG (↓)	Success	Avg.
PepGLAD	0.506	0.789	-21.94	55.97%	0.619
w/o Full-Atom	0.441	0.751	-20.87	51.18%	0.574
w/o Affine	0.450	0.740	-19.08	52.39%	0.564
w/o ProtFrag	0.535	0.760	-20.16	52.15%	0.597
w/o Mask	0.422	0.741	-20.45	57.44%	0.579

6. Conclusion

In this paper, we first assemble a dataset from Protein Data Bank (PDB) and literature to benchmark generative models on target-specific peptide design in terms of diversity, consistency, and binding energy. Subsequently, we propose PepGLAD, a powerful diffusion-based model for full-atom peptide design. In particular, we explore diffusion on the latent space where the sequence and the full-atom structure are jointly encoded by a variational autoencoder. We further propose a receptor-specific affine transformation technique to project variable geometries in the data space into a standard space, which enhances the transferability of diffusion processes on disparate binding sites. Our PepGLAD outperforms the existing models on sequence-structure co-design and binding conformation generation, exhibiting high generalization across diverse binding sites. Our work represents a pioneering effort in the

exploration of deep generative models for simultaneous design of 1D sequences and 3D structures of peptides, which could inspire future research in this field.

Impact Statements

This paper aims to advance the field of peptide design through the construction of a benchmark and the development of a novel latent diffusion model, PepGLAD, which addresses key limitations in current methods. Our work represents a step forward in computational peptide design, with the potential to impact both scientific research and practical applications in various domains. For instance, more precise peptide design could lead to enhanced drugs in the pharmaceutical industry, and could facilitate the creation of new biomaterials, sensors, and other innovative technologies in biology and materials science.

References

- Adolf-Bryfogle, J., Kalyuzhniy, O., Kubitz, M., Weitzner, B. D., Hu, X., Adachi, Y., Schief, W. R., and Dunbrack Jr, R. L. Rosettaantibodydesign (rabd): A general framework for computational antibody design. *PLoS computational biology*, 14(4):e1006112, 2018.
- Alford, R. F., Leaver-Fay, A., Jeliaskov, J. R., O’Meara, M. J., DiMaio, F. P., Park, H., Shapovalov, M. V., Renfrew, P. D., Mulligan, V. K., Kappel, K., et al. The rosetta all-atom energy function for macromolecular modeling and design. *Journal of chemical theory and computation*, 13(6):3031–3048, 2017.
- Anand, N. and Achim, T. Protein structure and sequence generation with equivariant denoising diffusion probabilistic models. *arXiv preprint arXiv:2205.15019*, 2022.
- Basu, S. and Wallner, B. Dockq: a quality measure for protein-protein docking models. *PloS one*, 11(8): e0161879, 2016.
- Berman, H. M., Westbrook, J., Feng, Z., Gilliland, G., Bhat, T. N., Weissig, H., Shindyalov, I. N., and Bourne, P. E. The protein data bank. *Nucleic acids research*, 28(1): 235–242, 2000.
- Bhardwaj, G., Mulligan, V. K., Bahl, C. D., Gilmore, J. M., Harvey, P. J., Cheneval, O., Buchko, G. W., Pulavarti, S. V., Kaas, Q., Eletsy, A., et al. Accurate de novo design of hyperstable constrained peptides. *Nature*, 538(7625):329–335, 2016.
- Bryant, P. and Elofsson, A. Evobind: in silico directed evolution of peptide binders with alphafold. *bioRxiv*, pp. 2022–07, 2022.
- Cao, L., Coventry, B., Goresnik, I., Huang, B., Sheffler, W., Park, J. S., Jude, K. M., Marković, I., Kadam, R. U., Verschuere, K. H., et al. Design of protein-binding proteins from the target structure alone. *Nature*, 605(7910):551–560, 2022.
- Chothia, C. and Janin, J. Principles of protein–protein recognition. *Nature*, 256(5520):705–708, 1975.
- Cock, P. J., Antao, T., Chang, J. T., Chapman, B. A., Cox, C. J., Dalke, A., Friedberg, I., Hamelryck, T., Kauff, F., Wilczynski, B., et al. Biopython: freely available python tools for computational molecular biology and bioinformatics. *Bioinformatics*, 25(11):1422, 2009.
- Cramér, H. *Mathematical methods of statistics*, volume 26. Princeton university press, 1999.
- Das, P., Sercu, T., Wadhawan, K., Padhi, I., Gehrman, S., Cipcigan, F., Chenthamarakshan, V., Strobel, H., Dos Santos, C., Chen, P.-Y., et al. Accelerated antimicrobial discovery via deep generative models and molecular dynamics simulations. *Nature Biomedical Engineering*, 5(6):613–623, 2021.
- Dauparas, J., Anishchenko, I., Bennett, N., Bai, H., Ragotte, R. J., Milles, L. F., Wicky, B. I., Courbet, A., de Haas, R. J., Bethel, N., et al. Robust deep learning–based protein sequence design using proteinmpnn. *Science*, 378(6615):49–56, 2022.
- Dhariwal, P. and Nichol, A. Diffusion models beat gans on image synthesis. *Advances in neural information processing systems*, 34:8780–8794, 2021.
- Duval, A., Mathis, S. V., Joshi, C. K., Schmidt, V., Miret, S., Malliaros, F. D., Cohen, T., Lio, P., Bengio, Y., and Bronstein, M. A hitchhiker’s guide to geometric gnns for 3d atomic systems. *arXiv preprint arXiv:2312.07511*, 2023.
- Fosgerau, K. and Hoffmann, T. Peptide therapeutics: current status and future directions. *Drug discovery today*, 20(1): 122–128, 2015.
- Golub, G. H. and Van Loan, C. F. *Matrix computations*. JHU press, 2013.
- Grathwohl, C. and Wüthrich, K. The x-pro peptide bond as an nmr probe for conformational studies of flexible linear peptides. *Biopolymers: Original Research on Biomolecules*, 15(10):2025–2041, 1976.
- Guruprasad, K., Reddy, B. B., and Pandit, M. W. Correlation between stability of a protein and its dipeptide composition: a novel approach for predicting in vivo stability of a protein from its primary sequence. *Protein Engineering, Design and Selection*, 4(2):155–161, 1990.

- Han, J., Rong, Y., Xu, T., and Huang, W. Geometrically equivariant graph neural networks: A survey. *arXiv preprint arXiv:2202.07230*, 2022.
- Henikoff, S. and Henikoff, J. G. Amino acid substitution matrices from protein blocks. *Proceedings of the National Academy of Sciences*, 89(22):10915–10919, 1992.
- Ho, J., Jain, A., and Abbeel, P. Denoising diffusion probabilistic models. *Advances in neural information processing systems*, 33:6840–6851, 2020.
- Hosseinzadeh, P., Watson, P. R., Craven, T. W., Li, X., Rettie, S., Pardo-Avila, F., Bera, A. K., Mulligan, V. K., Lu, P., Ford, A. S., et al. Anchor extension: a structure-guided approach to design cyclic peptides targeting enzyme active sites. *Nature Communications*, 12(1):3384, 2021.
- Ingraham, J., Garg, V., Barzilay, R., and Jaakkola, T. Generative models for graph-based protein design. *Advances in neural information processing systems*, 32, 2019.
- Ingraham, J. B., Baranov, M., Costello, Z., Barber, K. W., Wang, W., Ismail, A., Frappier, V., Lord, D. M., Ng-Thow-Hing, C., Van Vlack, E. R., et al. Illuminating protein space with a programmable generative model. *Nature*, pp. 1–9, 2023.
- Jin, W., Wohlwend, J., Barzilay, R., and Jaakkola, T. Iterative refinement graph neural network for antibody sequence-structure co-design. *arXiv preprint arXiv:2110.04624*, 2021.
- Jin, W., Barzilay, R., and Jaakkola, T. Antibody-antigen docking and design via hierarchical equivariant refinement. *arXiv preprint arXiv:2207.06616*, 2022.
- Jumper, J., Evans, R., Pritzel, A., Green, T., Figurnov, M., Ronneberger, O., Tunyasuvunakool, K., Bates, R., Žídek, A., Potapenko, A., et al. Highly accurate protein structure prediction with alphafold. *Nature*, 596(7873):583–589, 2021.
- Kingma, D. P. and Welling, M. Auto-encoding variational bayes. *arXiv preprint arXiv:1312.6114*, 2013.
- Kong, X., Huang, W., and Liu, Y. Conditional antibody design as 3d equivariant graph translation. *arXiv preprint arXiv:2208.06073*, 2022.
- Kong, X., Huang, W., and Liu, Y. End-to-end full-atom antibody design. *arXiv preprint arXiv:2302.00203*, 2023.
- Lee, A. C.-L., Harris, J. L., Khanna, K. K., and Hong, J.-H. A comprehensive review on current advances in peptide drug development and design. *International journal of molecular sciences*, 20(10):2383, 2019.
- Lei, Y., Li, S., Liu, Z., Wan, F., Tian, T., Li, S., Zhao, D., and Zeng, J. A deep-learning framework for multi-level peptide–protein interaction prediction. *Nature communications*, 12(1):5465, 2021.
- Leman, J. K., Weitzner, B. D., Lewis, S. M., Adolf-Bryfogle, J., Alam, N., Alford, R. F., Aprahamian, M., Baker, D., Barlow, K. A., Barth, P., et al. Macromolecular modeling and design in rosetta: recent methods and frameworks. *Nature methods*, 17(7):665–680, 2020.
- London, N., Movshovitz-Attias, D., and Schueler-Furman, O. The structural basis of peptide-protein binding strategies. *Structure*, 18(2):188–199, 2010.
- London, N., Raveh, B., Cohen, E., Fathi, G., and Schueler-Furman, O. Rosetta flexpepdock web server—high resolution modeling of peptide–protein interactions. *Nucleic acids research*, 39(suppl_2):W249–W253, 2011.
- Luo, S., Su, Y., Peng, X., Wang, S., Peng, J., and Ma, J. Antigen-specific antibody design and optimization with diffusion-based generative models for protein structures. *Advances in Neural Information Processing Systems*, 35: 9754–9767, 2022.
- Martinkus, K., Ludwiczak, J., Cho, K., Lian, W.-C., Lafrance-Vanasse, J., Hotzel, I., Rajpal, A., Wu, Y., Bonneau, R., Gligorijevic, V., et al. Abdiffuser: Full-atom generation of in-vitro functioning antibodies. *arXiv preprint arXiv:2308.05027*, 2023.
- Mitternacht, S. Freesasa: An open source c library for solvent accessible surface area calculations. *F1000Research*, 5, 2016.
- Muller, A. T., Hiss, J. A., and Schneider, G. Recurrent neural network model for constructive peptide design. *Journal of chemical information and modeling*, 58(2): 472–479, 2018.
- Needleman, S. B. and Wunsch, C. D. A general method applicable to the search for similarities in the amino acid sequence of two proteins. *Journal of molecular biology*, 48(3):443–453, 1970.
- Nichol, A. Q. and Dhariwal, P. Improved denoising diffusion probabilistic models. In *International Conference on Machine Learning*, pp. 8162–8171. PMLR, 2021.
- Rombach, R., Blattmann, A., Lorenz, D., Esser, P., and Ommer, B. High-resolution image synthesis with latent diffusion models. In *Proceedings of the IEEE/CVF conference on computer vision and pattern recognition*, pp. 10684–10695, 2022.

- Sohl-Dickstein, J., Weiss, E., Maheswaranathan, N., and Ganguli, S. Deep unsupervised learning using nonequilibrium thermodynamics. In *International conference on machine learning*, pp. 2256–2265. PMLR, 2015.
- Song, Y. and Ermon, S. Generative modeling by estimating gradients of the data distribution. *Advances in neural information processing systems*, 32, 2019.
- Steinegger, M. and Söding, J. Mmseqs2 enables sensitive protein sequence searching for the analysis of massive data sets. *Nature biotechnology*, 35(11):1026–1028, 2017.
- Swanson, S., Sivaraman, V., Grigoryan, G., and Keating, A. E. Tertiary motifs as building blocks for the design of protein-binding peptides. *Protein Science*, 31(6):e4322, 2022.
- Trippe, B. L., Yim, J., Tischer, D., Broderick, T., Baker, D., Barzilay, R., and Jaakkola, T. Diffusion probabilistic modeling of protein backbones in 3d for the motif-scaffolding problem. *arXiv preprint arXiv:2206.04119*, 2022.
- Tsaban, T., Varga, J. K., Avraham, O., Ben-Aharon, Z., Khramushin, A., and Schueler-Furman, O. Harnessing protein folding neural networks for peptide–protein docking. *Nature communications*, 13(1):176, 2022.
- Vanhee, P., van der Sloot, A. M., Verschueren, E., Serrano, L., Rousseau, F., and Schymkowitz, J. Computational design of peptide ligands. *Trends in biotechnology*, 29(5): 231–239, 2011.
- Verma, Y., Heinonen, M., and Garg, V. Abode: Ab initio antibody design using conjoined odes. *arXiv preprint arXiv:2306.01005*, 2023.
- Vincent, P., Larochelle, H., Lajoie, I., Bengio, Y., Manzagol, P.-A., and Bottou, L. Stacked denoising autoencoders: Learning useful representations in a deep network with a local denoising criterion. *Journal of machine learning research*, 11(12), 2010.
- Wang, D., Wen, Z., Ye, F., Zhou, H., and Li, L. Accelerating antimicrobial peptide discovery with latent sequence-structure model. *arXiv preprint arXiv:2212.09450*, 2022.
- Watson, J. L., Juergens, D., Bennett, N. R., Trippe, B. L., Yim, J., Eisenach, H. E., Ahern, W., Borst, A. J., Ragotte, R. J., Milles, L. F., et al. De novo design of protein structure and function with rfdiffusion. *Nature*, 620(7976): 1089–1100, 2023.
- Wen, Z., He, J., Tao, H., and Huang, S.-Y. Pepbdb: a comprehensive structural database of biological peptide–protein interactions. *Bioinformatics*, 35(1):175–177, 2019.
- Weng, G., Gao, J., Wang, Z., Wang, E., Hu, X., Yao, X., Cao, D., and Hou, T. Comprehensive evaluation of fourteen docking programs on protein–peptide complexes. *Journal of chemical theory and computation*, 16(6):3959–3969, 2020.
- Wu, K. E., Yang, K. K., van den Berg, R., Zou, J., Lu, A. X., and Amini, A. P. Protein structure generation via folding diffusion. 2022.
- Xia, H., McMichael, J., Becker-Hapak, M., Onyeador, O. C., Buchli, R., McClain, E., Pence, P., Supabphol, S., Richters, M. M., Basu, A., et al. Computational prediction of mhc anchor locations guides neoantigen identification and prioritization. *Science immunology*, 8(82):eabg2200, 2023.
- Xie, X., Valiente, P. A., and Kim, P. M. Helixgan a deep-learning methodology for conditional de novo design of α -helix structures. *Bioinformatics*, 39(1):btad036, 2023.
- Xie12, X., Valiente, P. A., Kim, J., and Kim123, P. M. Helixdiff: Hotspot-specific full-atom design of peptides using diffusion models.
- Xu, M., Yu, L., Song, Y., Shi, C., Ermon, S., and Tang, J. Geodiff: A geometric diffusion model for molecular conformation generation. *arXiv preprint arXiv:2203.02923*, 2022.
- Xu, M., Powers, A. S., Dror, R. O., Ermon, S., and Leskovec, J. Geometric latent diffusion models for 3d molecule generation. In *International Conference on Machine Learning*, pp. 38592–38610. PMLR, 2023.
- Yim, J., Trippe, B. L., De Bortoli, V., Mathieu, E., Doucet, A., Barzilay, R., and Jaakkola, T. Se (3) diffusion model with application to protein backbone generation. *arXiv preprint arXiv:2302.02277*, 2023.
- Zhang, Y., Zhang, Z., Zhong, B., Misra, S., and Tang, J. Diff-pack: A torsional diffusion model for autoregressive protein side-chain packing. *arXiv preprint arXiv:2306.01794*, 2023.

A. Reconstruction of Full-Atom Geometry

A.1. Auxiliary Loss for Training the AutoEncoder

To better recover the all-atom geometry, we employ an auxiliary structural loss similar to the violation loss in Jumper et al. (2021) including the supervision on C_α coordinates, bond lengths, and side-chain dihedral angles. First, since the C_α is critical in deciding the global geometry of the peptide, we exert additional loss on its coordinates to distinguish it from other atoms:

$$\mathcal{L}_{CA}(i) = \text{MSE}(\vec{r}_i, \vec{r}'_i), \quad (20)$$

where \vec{r}'_i and \vec{r}_i are the reconstructed and the ground truth coordinates of C_α in node i . Next, we implement L1 loss on the bond lengths:

$$\mathcal{L}_{bond}(i) = \sum_{b \in \mathcal{B}(i)} |b - b'|/|\mathcal{B}(i)|, \quad (21)$$

where $\mathcal{B}(i)$ includes all chemical bonds in node i , and b' denotes the reconstructed bond length. For simplicity, the bonds between residues are included into the bonds of the former residue. Finally, we supervise on the χ_1 to χ_4 side-chain dihedral angles (Zhang et al., 2023):

$$\mathcal{L}_{angle}(i) = \sum_{\chi \in \mathcal{A}(i)} |\chi - \chi'|/|\mathcal{A}(i)|, \quad (22)$$

where $\mathcal{A}(i)$ includes all side-chain dihedral angles in node i , χ' and χ denotes the reconstructed and the ground truth angles, respectively. The overall auxiliary loss for node i is then given by:

$$\mathcal{L}_{aux}(i) = \lambda_{CA}\mathcal{L}_{CA}(i) + \lambda_{bond}\mathcal{L}_{bond}(i) + \lambda_{angle}\mathcal{L}_{angle}(i), \quad (23)$$

where we set $\lambda_{CA} = 1.0$, $\lambda_{bond} = 1.0$, $\lambda_{angle} = 0.5$ in our experiments. We find that it is necessary to set λ_{angle} with a relatively small value to make the training process stable.

A.2. Idealization of Local Geometry

Preserving atom instances enhances the modeling of side chain interactions but introduces challenges due to potential twisting in local geometry. While in sequence-structure co-design, samples undergo fast relax by physical force field to ensure a valid local geometry, in binding conformation generation, we use an alignment technique to place the idealized side chains on the generated atom instances. Specifically, the idealized side chain can be represented as at most 4 dihedral angles (χ -angles), treating fragments like phenyl group as rigid bodies. Suppose there are n_i χ -angles and c_i atoms in node i , we can define a function to map from the χ -angles with the backbone coordinates $\vec{B}_i \in \mathbb{R}^{4 \times 3}$ to atom instances as $M_i : \mathbb{R}^{n_i} \times \mathbb{R}^{4 \times 3} \rightarrow \mathbb{R}^{c_i \times 3}$, which is luckily differentiable (Ingraham et al., 2023). Thus we can optimize χ -angles via gradient descent to minimize the MSE between the coordinates constructed from χ -angles and those generated by the model:

$$\chi_i^* = \arg \min_{\chi \in [0, 2\pi]^{n_i}} \|M_i(\chi, \vec{B}_i) - \vec{X}_i\|^2, \quad (24)$$

where $\vec{X}_i \in \mathbb{R}^{c_i \times 3}$ denotes the coordinates of c_i atom instances in node i generated by the model. Now it should be easy to construct an idealized side chain maintaining fidelity to the generated atom instances by $M(\chi_i^*, \vec{B}_i)$.

B. Proof of Proposition 3.1

Proposition 3.1. *Denote the invariant and equivariant outputs from a scalarization-based $E(3)$ -equivariant GNN as $f(\{\mathbf{h}_i, \vec{\mathbf{x}}_i\})$ and $\tilde{f}(\{\mathbf{h}_i, \vec{\mathbf{x}}_i\})$, respectively. With the definition of F in Eq. 9, $\forall g \in E(3)$, we have $f(\{\mathbf{h}_i, F(\vec{\mathbf{x}}_i)\}) = f(\{\mathbf{h}_i, F_g(g \cdot \vec{\mathbf{x}}_i)\})$ and $g \cdot F^{-1}(\tilde{f}(\{\mathbf{h}_i, F(\vec{\mathbf{x}}_i)\})) = F_g^{-1}(\tilde{f}(\{\mathbf{h}_i, F_g(g \cdot \vec{\mathbf{x}}_i)\}))$, where F_g is derived on the coordinates transformed by g . Namely, the $E(3)$ -equivariance is preserved if we implement the GNN on the standard space and recover the original geometry from the outputs.*

For simplicity, given F derived from a set of coordinates $\{\vec{\mathbf{x}}_i\}$ following Eq. 9, we use F_g to indicate the affine transformation derived from $\{g \cdot \vec{\mathbf{x}}_i\}$, where $g \in E(3)$. Additionally, we keep the terminology "standard space" for describing the space after the data-specific affine transformation F . We begin by proving a key lemma, that is, the $E(3)$ -invariance of distances between two nodes in the standard space converted by F :

Lemma C.1. Given two nodes i and j in the geometric graph \mathcal{G} , denoting their coordinates as \vec{x}_i and \vec{x}_j , their distance in the standard space is $E(3)$ -invariant. Namely, $\forall g \in E(3)$, $\|F(\vec{x}_i) - F(\vec{x}_j)\| = \|F_g(g \cdot \vec{x}_i) - F_g(g \cdot \vec{x}_j)\|$.

Proof. $\forall g \in E(3)$, g can be instantiated as an orthogonal matrix $\mathbf{Q} \in O(3)$ (including rotation and reflection), and a translation vector $\vec{t} \in \mathbb{R}^3$. Denoting all coordinates in the geometric graph as $\vec{\mathbf{X}} \in \mathbb{R}^{3 \times |\mathcal{G}|}$, and the number of nodes in \mathcal{G} as n , we can derive the $E(3)$ -equivariance of the expectation of the coordinates:

$$\mathbb{E}[g \cdot \vec{\mathbf{X}}] = \frac{1}{n} \sum_i g \cdot \vec{x}_i = \frac{1}{n} \sum_i (\mathbf{Q}\vec{x}_i + \vec{t}) \quad (25)$$

$$= \frac{1}{n} \mathbf{Q} \left(\sum_i \vec{x}_i \right) + \vec{t} = \mathbf{Q} \mathbb{E}[\vec{\mathbf{X}}] + \vec{t} \quad (26)$$

$$= g \cdot \mathbb{E}[\vec{\mathbf{X}}]. \quad (27)$$

With the $E(3)$ -equivariance of the expectation, it is easy to derive the following equation on the covariance matrix:

$$\text{Cov}(g \cdot \vec{\mathbf{X}}, g \cdot \vec{\mathbf{X}}) = \frac{1}{n-1} (g \cdot \vec{\mathbf{X}} - \mathbb{E}[g \cdot \vec{\mathbf{X}}]) (g \cdot \vec{\mathbf{X}} - \mathbb{E}[g \cdot \vec{\mathbf{X}}])^\top \quad (28)$$

$$= \frac{1}{n-1} (g \cdot \vec{\mathbf{X}} - g \cdot \mathbb{E}[\vec{\mathbf{X}}]) (g \cdot \vec{\mathbf{X}} - g \cdot \mathbb{E}[\vec{\mathbf{X}}])^\top \quad (29)$$

$$= \frac{1}{n-1} (\mathbf{Q}(\vec{\mathbf{X}} - \mathbb{E}[\vec{\mathbf{X}}])) (\mathbf{Q}(\vec{\mathbf{X}} - \mathbb{E}[\vec{\mathbf{X}}]))^\top \quad (30)$$

$$= \frac{1}{n-1} \mathbf{Q}(\vec{\mathbf{X}} - \mathbb{E}[\vec{\mathbf{X}}]) (\vec{\mathbf{X}} - \mathbb{E}[\vec{\mathbf{X}}])^\top \mathbf{Q}^\top \quad (31)$$

$$= \mathbf{Q} \text{Cov}(\vec{\mathbf{X}}, \vec{\mathbf{X}}) \mathbf{Q}^\top. \quad (32)$$

Based on the Cholesky decomposition used in the derivation of F , we denote $\text{Cov}(\vec{\mathbf{X}}, \vec{\mathbf{X}}) = \vec{\mathbf{L}}\vec{\mathbf{L}}^\top$ and $\text{Cov}(g \cdot \vec{\mathbf{X}}, g \cdot \vec{\mathbf{X}}) = \vec{\mathbf{L}}_g \vec{\mathbf{L}}_g^\top$, with which we can immediately derive:

$$\vec{\mathbf{L}}_g \vec{\mathbf{L}}_g^\top = \mathbf{Q} \vec{\mathbf{L}} \vec{\mathbf{L}}^\top \mathbf{Q}^\top. \quad (33)$$

Considering $\mathbf{Q}^{-1} = \mathbf{Q}^\top$, we further have the following equation:

$$\vec{\mathbf{L}}_g^{-\top} \vec{\mathbf{L}}_g^{-1} = \mathbf{Q} \vec{\mathbf{L}}^{-\top} \vec{\mathbf{L}}^{-1} \mathbf{Q}^\top. \quad (34)$$

Given that $F(\vec{x}) = \vec{\mathbf{L}}^{-1}(\vec{x} - \mathbb{E}[\vec{\mathbf{X}}])$, we are now ready to prove Lemma C.1 as follows:

$$\|F_g(g \cdot \vec{x}_i) - F_g(g \cdot \vec{x}_j)\| = \|\vec{\mathbf{L}}_g^{-1}(g \cdot \vec{x}_i - \mathbb{E}[g \cdot \vec{\mathbf{X}}]) - \vec{\mathbf{L}}_g^{-1}(g \cdot \vec{x}_j - \mathbb{E}[g \cdot \vec{\mathbf{X}}])\| = \|\vec{\mathbf{L}}_g^{-1}(g \cdot \vec{x}_i - g \cdot \vec{x}_j)\| \quad (35)$$

$$= \|\vec{\mathbf{L}}_g^{-1} \mathbf{Q}(\vec{x}_i - \vec{x}_j)\| = \sqrt{(\vec{\mathbf{L}}_g^{-1} \mathbf{Q}(\vec{x}_i - \vec{x}_j))^\top (\vec{\mathbf{L}}_g^{-1} \mathbf{Q}(\vec{x}_i - \vec{x}_j))} \quad (36)$$

$$= \sqrt{(\vec{x}_i - \vec{x}_j)^\top \mathbf{Q}^\top \vec{\mathbf{L}}_g^{-\top} \vec{\mathbf{L}}_g^{-1} \mathbf{Q}(\vec{x}_i - \vec{x}_j)} = \sqrt{(\vec{x}_i - \vec{x}_j)^\top \vec{\mathbf{L}}^{-\top} \vec{\mathbf{L}}^{-1}(\vec{x}_i - \vec{x}_j)} \quad (37)$$

$$= \sqrt{(\vec{\mathbf{L}}^{-1}(\vec{x}_i - \vec{x}_j))^\top (\vec{\mathbf{L}}^{-1}(\vec{x}_i - \vec{x}_j))} = \|\vec{\mathbf{L}}^{-1}(\vec{x}_i - \vec{x}_j)\| \quad (38)$$

$$= \|\vec{\mathbf{L}}^{-1}(\vec{x}_i - \mathbb{E}[\vec{\mathbf{X}}]) - \vec{\mathbf{L}}^{-1}(\vec{x}_j - \mathbb{E}[\vec{\mathbf{X}}])\| = \|F(\vec{x}_i) - F(\vec{x}_j)\| \quad (39)$$

□

With Lemma C.1, we are able to give the proof of Proposition 3.1 as follows.

Proof. A first observation is that to prove Proposition 3.1, we only need to prove the equivariance in the 1-layer case, since the multi-layer case can be decomposed into the 1-layer case by inserting $I = F \circ F^{-1}$ between layers, where I is the

identical mapping. Generally, each layer in scalarization-based E(3)-equivariant GNN has the following paradigm:

$$\mathbf{m}_{ij} = \phi_m(\mathbf{h}_i, \mathbf{h}_j, \|\vec{\mathbf{x}}_i - \vec{\mathbf{x}}_j\|^2, \mathbf{e}_{ij}), \quad (40)$$

$$\vec{\mathbf{x}}'_i = \vec{\mathbf{x}}_i + \sum_{j \in \mathcal{N}(i)} (\vec{\mathbf{x}}_i - \vec{\mathbf{x}}_j) \phi_x(\mathbf{m}_{ij}), \quad (41)$$

$$\vec{\mathbf{h}}'_i = \phi_h(\mathbf{h}_i, \sum_{j \in \mathcal{N}(i)} \mathbf{m}_{ij}), \quad (42)$$

where $\mathcal{N}(i)$ denotes the neighborhood of node i , and ϕ_x outputs a scalar. Therefore, for the invariant part, we have:

$$f_i(\{\mathbf{h}_i, F_g(g \cdot \vec{\mathbf{x}}_i)\}) = \phi_h(\mathbf{h}_i, \sum_{j \in \mathcal{N}(i)} \mathbf{m}_{ij, F_g}) \quad (43)$$

$$= \phi_h(\mathbf{h}_i, \sum_{j \in \mathcal{N}(i)} \phi_m(\mathbf{h}_i, \mathbf{h}_j, \|F_g(g \cdot \vec{\mathbf{x}}_i) - F_g(g \cdot \vec{\mathbf{x}}_j)\|^2, \mathbf{e}_{ij})) \quad (44)$$

$$= \phi_h(\mathbf{h}_i, \sum_{j \in \mathcal{N}(i)} \phi_m(\mathbf{h}_i, \mathbf{h}_j, \|F(\vec{\mathbf{x}}_i) - F(\vec{\mathbf{x}}_j)\|^2, \mathbf{e}_{ij})) \quad (45)$$

$$= \phi_h(\mathbf{h}_i, \sum_{j \in \mathcal{N}(i)} \mathbf{m}_{ij, F}) \quad (46)$$

$$= f_i(\{\mathbf{h}_i, F(\vec{\mathbf{x}}_i)\}) \quad (47)$$

For the equivariant features, recalling $F^{-1}(\vec{\mathbf{x}}) = \vec{\mathbf{L}}\vec{\mathbf{x}} + \mathbb{E}[\vec{\mathbf{X}}]$, we have:

$$F_g^{-1} \vec{f}_i(\{\mathbf{h}_i, F_g(g \cdot \vec{\mathbf{x}}_i)\}) = F_g^{-1}(F_g(g \cdot \vec{\mathbf{x}}_i) + \sum_{j \in \mathcal{N}(i)} (F_g(g \cdot \vec{\mathbf{x}}_i) - F_g(g \cdot \vec{\mathbf{x}}_j)) \phi_x(\mathbf{m}_{ij, F_g})) \quad (48)$$

$$= F_g^{-1}(F_g(g \cdot \vec{\mathbf{x}}_i) + \sum_{j \in \mathcal{N}(i)} \vec{\mathbf{L}}_g^{-1} \mathbf{Q}(\vec{\mathbf{x}}_i - \vec{\mathbf{x}}_j) \phi_x(\mathbf{m}_{ij, F})) \quad (49)$$

$$= F_g^{-1}(\vec{\mathbf{L}}_g^{-1}(\mathbf{Q}\vec{\mathbf{x}}_i + \vec{\mathbf{t}} - \mathbb{E}[g \cdot \vec{\mathbf{X}}]) + \sum_{j \in \mathcal{N}(i)} \vec{\mathbf{L}}_g^{-1} \mathbf{Q}(\vec{\mathbf{x}}_i - \vec{\mathbf{x}}_j) \phi_x(\mathbf{m}_{ij, F})) \quad (50)$$

$$= F_g^{-1}(\vec{\mathbf{L}}_g^{-1}(\mathbf{Q}\vec{\mathbf{x}}_i + \vec{\mathbf{t}} - g \cdot \mathbb{E}[\vec{\mathbf{X}}]) + \sum_{j \in \mathcal{N}(i)} \vec{\mathbf{L}}_g^{-1} \mathbf{Q}(\vec{\mathbf{x}}_i - \vec{\mathbf{x}}_j) \phi_x(\mathbf{m}_{ij, F})) \quad (51)$$

$$= F_g^{-1}(\vec{\mathbf{L}}_g^{-1}(\mathbf{Q}\vec{\mathbf{x}}_i - \mathbf{Q}\mathbb{E}[\vec{\mathbf{X}}]) + \sum_{j \in \mathcal{N}(i)} \vec{\mathbf{L}}_g^{-1} \mathbf{Q}(\vec{\mathbf{x}}_i - \vec{\mathbf{x}}_j) \phi_x(\mathbf{m}_{ij, F})) \quad (52)$$

$$= F_g^{-1}(\vec{\mathbf{L}}_g^{-1} \mathbf{Q}(\vec{\mathbf{x}}_i - \mathbb{E}[\vec{\mathbf{X}}]) + \sum_{j \in \mathcal{N}(i)} \vec{\mathbf{L}}_g^{-1} \mathbf{Q}(\vec{\mathbf{x}}_i - \vec{\mathbf{x}}_j) \phi_x(\mathbf{m}_{ij, F})) \quad (53)$$

$$= F_g^{-1}(\vec{\mathbf{L}}_g^{-1} \mathbf{Q}(\vec{\mathbf{x}}_i - \mathbb{E}[\vec{\mathbf{X}}]) + \sum_{j \in \mathcal{N}(i)} (\vec{\mathbf{x}}_i - \vec{\mathbf{x}}_j) \phi_x(\mathbf{m}_{ij, F})) \quad (54)$$

$$= \mathbf{Q}(\vec{\mathbf{x}}_i - \mathbb{E}[\vec{\mathbf{X}}]) + \sum_{j \in \mathcal{N}(i)} (\vec{\mathbf{x}}_i - \vec{\mathbf{x}}_j) \phi_x(\mathbf{m}_{ij, F}) + \mathbb{E}[g \cdot \vec{\mathbf{X}}] \quad (55)$$

$$= \mathbf{Q}(\vec{\mathbf{x}}_i + \sum_{j \in \mathcal{N}(i)} (\vec{\mathbf{x}}_i - \vec{\mathbf{x}}_j) \phi_x(\mathbf{m}_{ij, F})) - \mathbf{Q}\mathbb{E}[\vec{\mathbf{X}}] + g \cdot \mathbb{E}[\vec{\mathbf{X}}] \quad (56)$$

$$= \mathbf{Q}(\vec{\mathbf{x}}_i + \sum_{j \in \mathcal{N}(i)} (\vec{\mathbf{x}}_i - \vec{\mathbf{x}}_j) \phi_x(\mathbf{m}_{ij, F})) + \vec{\mathbf{t}} \quad (57)$$

$$= g \cdot (\vec{\mathbf{x}}_i + \sum_{j \in \mathcal{N}(i)} (\vec{\mathbf{x}}_i - \vec{\mathbf{x}}_j) \phi_x(\mathbf{m}_{ij, F})) \quad (58)$$

By replacing g with identical element I in $E(3)$, since $F = F_I$, we can immediately derive:

$$F^{-1} \vec{f}_i(\{\mathbf{h}_i, F(\vec{\mathbf{x}}_i)\}) = (\vec{\mathbf{x}}_i + \sum_{j \in \mathcal{N}(i)} (\vec{\mathbf{x}}_i - \vec{\mathbf{x}}_j) \phi_x(\mathbf{m}_{ij, F})), \quad (59)$$

$$g \cdot F^{-1} \vec{f}_i(\{\mathbf{h}_i, F(\vec{\mathbf{x}}_i)\}) = F_g^{-1} \vec{f}_i(\{\mathbf{h}_i, F_g(g \cdot \vec{\mathbf{x}}_i)\}), \quad (60)$$

which concludes Proposition 3.1. \square

D. Data Preparation

D.1. Unsupervised Data from Protein Fragments (ProtFrag)

We exploit unsupervised data from monomer proteins to enrich the training of the autoencoder. Specifically, we first extract all single chains from the Protein Data Bank (PDB) before December 8th, 2023, and remove the duplicated chains on a sequence identity threshold of over 90%. Then, for each chain, we extract fragments satisfying the following criteria:

1. **Length:** The fragment should consist of 4 to 25 residues.
2. **Balanced constitution:** No single amino acid should constitute more than 25% of the fragment; Hydrophobic amino acids should comprise less than 45% of the fragment, with charged amino acids accounting for 25% to 45%.
3. **Isolated Stability:** Instability (Guruprasad et al., 1990) should be below 40; Considering the surrounding amino acids as interaction partners, the fragment should have a buried surface area (BSA) above 400\AA^2 (Chothia & Janin, 1975), with a relative BSA above 20%.

We use FreeSASA (Mitternacht, 2016) to calculate the surface area of fragments. Let SA_{bound} represent the surface area of the isolated fragment when considering surrounding amino acids, and $SA_{unbound}$ represent the surface area when not considering them. The buried surface area is then calculated as $BSA = SA_{unbound} - SA_{bound}$, and the relative BSA is calculated as $BSA_{rel} = BSA/SA_{unbound}$. In total, we obtain 70,645 fragments meeting these criteria.

D.2. Dataset of Protein-Peptide Complexes

Here we illustrate the details for constructing the supervised dataset used in our paper. Similar to literature (Wen et al., 2019), we also exploits available data from the Protein Data Bank (PDB) (Berman et al., 2000). We first extract all dimers in PDB deposited before December 8th, 2023, and filter out the complexes with a receptor longer than 30 residues and a ligand between 4 to 25 residues, which aligns with Tsaban et al. (2022). Then we remove the duplicated complexes with the criterion that both the receptor and the peptide has a sequence identity over 90% (Steinegger & Söding, 2017), after which 6105 non-redundant complexes are obtained. We use MMseqs2 for clustering based on sequence identity:

```
# create database from the sequences
mmseqs create seqs.fasta database
# clustering with sequence identity above 90%
mmseqs cluster database database_clusters results --min-seq-id 0.9 -c 0.95 --cov-mode 1
```

To achieve the cross-target generalization test, we utilize the large non-redundant dataset (LNR) introduced by Tsaban et al. (2022) as the test set, which is curated by domain experts. LNR originally includes 96 protein-peptide complexes. We obtain 93 complexes after excluding the ones with non-canonical amino acids. We then cluster the LNR along with the PDB data by receptor with a sequence identity threshold of over 40%. Subsequently, we remove the complexes sharing the same clusters with those from the test set and those including non-canonical amino acids in the peptides. Finally, the remaining data are randomly split based on clustering results into training and validation sets. The characteristics of different splits are presented in Table 1. In addition, the binding site contains residues on the receptor within 10\AA distances to the peptide, where the distance between two residues is measured by the distance between their C_β coordinates.

E. Guidance on Sequence Orders for Sampling

Peptides consist of linearly connected amino acids, which exert constraints on the 3D geometry. Specifically, residues adjacent in the sequence should also be close in the structure, since they are connected by a peptide bond. However, 3D graphs are unordered and do not incorporate such induct bias, which means the generated nodes might have arbitrary permutation on sequence orders. To tackle this problem, we take inspiration from classifier-guided diffusion (Dhariwal & Nichol, 2021), which adds the gradient of a classifier to the denoising outputs to guide the generative diffusion process towards the subspace where the classifier gives high confidence. We utilize an empirical classifier $p(1|\{\mathbf{z}_i^t\})$ defined as follows:

$$p(1|\{\mathbf{z}_i^t\}) = \exp(-\sum_{\mathcal{P}(i)-\mathcal{P}(j)=1} E(\|\mathbf{z}_i^t - \mathbf{z}_j^t\|)), \quad (61)$$

$$E(d) = \begin{cases} d - (\mu_d + 3\sigma_d), & d > \mu_d + 3\sigma_d, \\ (\mu_d - 3\sigma_d) - d, & d < \mu_d - 3\sigma_d, \\ 0, & \text{otherwise,} \end{cases} \quad (62)$$

where μ_d and σ_d are the mean and variance of the distances of adjacent residues in the latent space measured from the training set. With $p(1|\{\mathbf{z}_i^t\})$, we are able to assign an arbitrary permutation on sequence orders to the nodes, and steer the sampling procedure towards the desired subspace conforming to \mathcal{P} , since this classifier gives higher confidence if the adjacent (defined by \mathcal{P}) residues are within reasonable distances aligning with the statistics from the training set. In particular, the coordinate denoising outputs are refined as follows:

$$\tilde{\mathbf{e}}_i^t = \tilde{\mathbf{e}}_\theta(\mathcal{G}_z^t, \mathcal{G}_b, t)[i] - \lambda\sqrt{1 - \bar{\alpha}^t}\nabla_{\mathbf{z}_i^t} \log p(1|\{\mathbf{z}_i^t\}), \quad (63)$$

where λ adjusts the weight of the guidance. Besides the constraints on the distance between adjacent residues, we can also include guidance on avoiding clashes between non-adjacent residues by defining the following energy term:

$$C(d) = \begin{cases} \mu_d - d, & d < \mu_d, \\ 0, & \text{otherwise,} \end{cases} \quad (64)$$

Subsequently, we just need to revise the empirical classifier as:

$$p(1|\{\bar{z}_i^t\}) = \exp(-\sum_{\mathcal{P}(i)-\mathcal{P}(j)=1} E(\|\bar{z}_i^t - \bar{z}_j^t\|) - \sum_{\mathcal{P}(i)-\mathcal{P}(j)\neq 1} C(\|\bar{z}_i^t - \bar{z}_j^t\|) - \sum_{i \in \mathcal{G}_z, j \in \mathcal{G}_b} C(\|\bar{z}_i^t - \bar{r}_j\|), \quad (65)$$

where \bar{r}_j is the C_α coordinate of node j in the binding site. We observe a slight improvement upon including the clash energy term.

F. Metrics for Evaluating Sequence-Structure Co-Design

F.1. Why not Amino Acid Recovery (AAR)

While the amino acid recovery (AAR) is widely used in antibody design (Kong et al., 2022; 2023; Luo et al., 2022), we find it not informative enough for evaluating generative models on learning the distribution of binding peptides, due to the vast and highly diverse solution space. To elucidate this, we conducted an analysis of AAR using a sequence dataset from Xia et al. (2023) including 328 receptors and 600k peptides with binary binding labels, from which we filter out 102 receptors with well-explored solution space (*i.e.* with at least 500 binders). For each receptor, we randomly select one binder as the reference and sample N candidates according to a specified positive ratio r , resembling the scenario of evaluating generative models for peptide design. For example, setting $r = 0.1$ and $N = 100$ involves sampling 10 binders and 90 non-binders to construct the candidates. Then we compute the best AAR of these candidates with respect to the reference as the result. This process is repeated for 10 times per receptor, and the results are averaged across different receptors, which can be interpreted as the evaluation score of AAR on a generative model that can generate candidates with a positive ratio of r . We select $N = 10, 40, 100$ and enumerate the choices of r to derive the relation plot in Figure 6, where the results of a random sequence generator is also included for comparison. It can be derived that the gap of AAR between the worst model ($r = 0.0$) and the best model ($r = 1.0$) is insignificant. Furthermore, all models, including the best model ($r = 1.0$) which always produces positive samples, exhibit performance akin to the random sequence generator, with consistent trends regardless of the choice of N . We attribute this to the vast solution space of peptide design, where evaluating with dozens of candidates relative to a single reference is unreliable. In other words, **achieving a high AAR is improbable since the model would need to fortuitously explore the subspace around the reference, which is arbitrary, on every test receptor; Conversely, a low AAR does not necessarily denote a poor generative model, as the model may be exploring distinct solutions from the single reference.** Moreover, we calculate the Spearman correlation between the receptor-level best AAR and the positive ratio r of the candidates, yielding 0.23, 0.22 and 0.24 for $N = 10, 40$, and 100, respectively, indicating very weak correlation. Based on this analysis, we assert that AAR is unsuitable for evaluating target-specific peptide design.

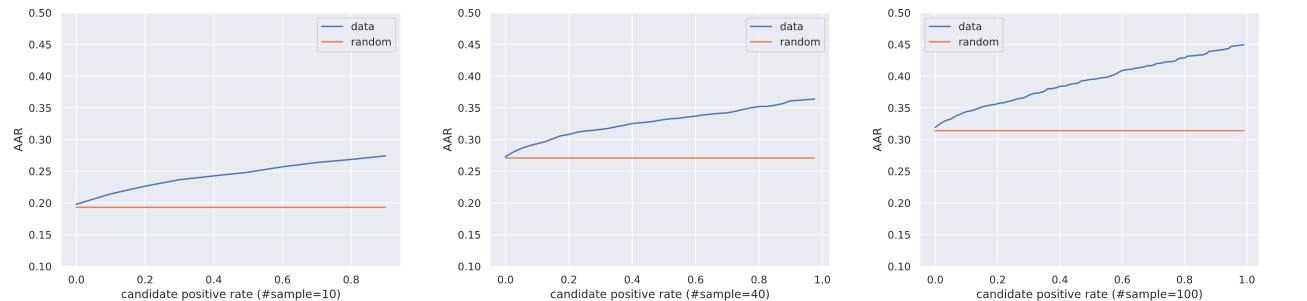


Figure 6. Best amino acid recovery (AAR) on samples constructed according to specified positive ratios. Each point contains the averaged result across 102 receptors.

F.2. Implementation and Discussion on Metrics

Indeed, evaluating generative models comprehensively is crucial, requiring assessment from multiple perspectives. Generally, these evaluations can be categorized into two main aspects: diversity and fidelity to the desired distribution. Regarding diversity, we take inspiration from [Yim et al. \(2023\)](#) and quantify it with the number of unique clusters relative to the number of candidates. This metric provides insight into the variety and richness of the generated samples. For fidelity, the primary focus should be the binding affinity, for which we adopt the physical energy from Rosetta ([Alford et al., 2017](#)) since it is widely used in various domains and exhibit robust generalization capability ([Adolf-Bryfogle et al., 2018](#); [Leman et al., 2020](#); [Watson et al., 2023](#)). Further, considering the dependency between sequence and structure, we propose the consistency metric, which is critical for distinguishing whether the generative model is capturing the 1D&3D joint distribution and thereby truly facilitating "co-design". Below, we outline the implementation of these metrics.

Diversity We hierarchically cluster the sequences and the structures with aligning score ([Lei et al., 2021](#)) and RMSD of C_α , respectively. In particular, we implement the aligning score using Biopython ([Cock et al., 2009](#)) with BLOSUM62 matrix ([Henikoff & Henikoff, 1992](#)) and Needleman-Wunsch algorithm ([Needleman & Wunsch, 1970](#)). The thresholds for clustering is similarity above 0.6 and RMSD below 4.0 for sequence and structure, respectively. We provide the python codes below for clearer presentation:

```
from math import sqrt
from typing import List
from Bio.Align import substitution_matrices, PairwiseAligner

import numpy as np

def align_score(sequence_A, sequence_B):
    # load matrix
    sub_matrice = substitution_matrices.load('BLOSUM62')
    aligner = PairwiseAligner()
    aligner.substitution_matrix = sub_matrice
    # align
    alns = aligner.align(sequence_A, sequence_B)
    best_aln = alns[0]
    aligned_A, aligned_B = best_aln
    # normalize
    base_A = aligner.score(sequence_A, sequence_A)
    base_B = aligner.score(sequence_B, sequence_B)
    base = sqrt(base_A * base_B)
    similarity = aligner.score(sequence_A, sequence_B) / base
    return similarity

def seq_diversity(seqs: List[str], th: float=0.4) -> float:
    """
    th: sequence distance (1 - similarity)
    """
    dists = []
    for i, sequence_A in enumerate(seqs):
        dists.append([])
        for j, sequence_B in enumerate(seqs):
            dists[i].append(1 - align_score(sequence_A, sequence_B))
    dists = np.array(dists)
    Z = linkage(squareform(dists), 'single')
    cluster = fcluster(Z, t=th, criterion='distance')
    return len(np.unique(cluster)) / len(seqs)

def struct_diversity(structs: np.ndarray, th: float=4.0) -> float:
    """
    structs: N*L*3, alpha carbon coordinates
    th: threshold for clustering (distance < th)
    """
    ca_dists = np.sum((structs[:, None] - structs[None, :]) ** 2, axis=-1)
    rmsd = np.sqrt(np.mean(ca_dists, axis=-1))
    Z = linkage(squareform(rmsd), 'single')
    cluster = fcluster(Z, t=th, criterion='distance')
    return len(np.unique(cluster)) / structs.shape[0]
```

Denoting the diversity of the sequences and the structures as Div_{seq} and Div_{struct} , respectively, we calculate the co-design diversity as $\sqrt{Div_{seq} Div_{struct}}$.

Consistency The clustering process in the calculation of diversity will assign each sequence and each structure with a clustering label. The labels on the sequences and those on the structures can be regarded as two nominal variables. Since similar sequences should produce similar structures, these two variables should be highly correlated if the model really learns the joint distribution. Naturally, we quantify the consistency via Cramér’s V (Cramér, 1999) association between these two variables, with 1.0 indicating perfect association, and 0.0 means no association.

ΔG We use Rosetta (Alford et al., 2017) to calculate the binding energy with the "ref2015" score function. Both the candidates and the references first endure the fast relax protocol in Rosetta to correct atomic clashes at the interface before the computation of binding energy. We use the implementation in pyRosetta (*i.e.* the python version of Rosetta), which is borrowed from Luo et al. (2022):

```
import pyrosetta
from pyrosetta.rosetta import protocols
from pyrosetta.rosetta.protocols.relax import FastRelax
from pyrosetta.rosetta.core.pack.task import TaskFactory
from pyrosetta.rosetta.core.pack.task import operation
from pyrosetta.rosetta.core.select import residue_selector as selections
from pyrosetta.rosetta.core.select.movemap import MoveMapFactory, move_map_action
from pyrosetta.rosetta.core.scoring import ScoreType
from pyrosetta.rosetta.protocols.analysis import InterfaceAnalyzerMover

pyrosetta.init(' '.join([
    '-mute', 'all',
    '-use_input_sc',
    '-ignore_unrecognized_res',
    '-ignore_zero_occupancy', 'false',
    '-load_PDB_components', 'false',
    '-relax:default_repeats', '2',
    '-no_fconfig',
    '-use_terminal_residues', 'true',
    '-in:file:silent_struct_type', 'binary'
]))

class RelaxRegion(object): # Fast Relax

    def __init__(self, max_iter=1000):
        super().__init__()
        self.scorefxn = pyrosetta.create_score_function('ref2015')
        self.fast_relax = FastRelax()
        self.fast_relax.set_scorefxn(self.scorefxn)
        self.fast_relax.max_iter(max_iter)

    def __call__(self, pdb_path, peptide_chain):
        pose = pyrosetta.pose_from_pdb(pdb_path)

        tf = TaskFactory()
        tf.push_back(operation.InitializeFromCommandline())
        tf.push_back(operation.RestrictToRepacking()) # Only allow residues to repack. No design at any position.

        gen_selector = selections.ChainSelector(chain)
        nbr_selector = selections.NeighborhoodResidueSelector()
        nbr_selector.set_focus_selector(gen_selector)
        nbr_selector.set_include_focus_in_subset(True)
        subset_selector = nbr_selector

        prevent_repacking_rlt = operation.PreventRepackingRLT()
        prevent_subset_repacking = operation.OperateOnResidueSubset(
            prevent_repacking_rlt,
            subset_selector,
            flip_subset=True,
        )
        tf.push_back(prevent_subset_repacking)

        fr = self.fast_relax
        pose = original_pose.clone()

        mmf = MoveMapFactory()
        mmf.add_bb_action(move_map_action.mm_enable, gen_selector)
        mmf.add_chi_action(move_map_action.mm_enable, subset_selector)
        mm = mmf.create_movemap_from_pose(pose)

        fr.set_movemap(mm)
        fr.set_task_factory(tf)
        fr.apply(pose)

        return pose
```

```
def pyrosetta_interface_energy(pdb_path, receptor_chains, ligand_chains): # binding energy
    pose = pyrosetta.pose_from_pdb(pdb_path)
    interface = ''.join(ligand_chains) + '_' + ''.join(receptor_chains)
    mover = InterfaceAnalyzerMover(interface)
    mover.set_pack_separated(True)
    mover.apply(pose)
    return pose.scores['dG_separated']
```

Success Since a negative ΔG value typically indicates a potential for binding, we report the ratio of all generated candidates that satisfy this threshold.

G. Experiment Details

G.1. Implementation of PepGLAD

We train PepGLAD on a GPU with 24G memory with AdamW optimizer. For the autoencoder, we train for 60 epochs with dynamic batches, ensuring that the total number of edges (proportional to the square of the number of nodes) remains below 60,000. The initial learning rate is 10^{-4} and decays by 0.8 if the loss on the validation set has not decreased for 3 consecutive epochs. Regarding the diffusion model, we train for 500 epochs with the same batching strategy as for the autoencoder. The learning rate is 10^{-4} and decay by 0.6 if the loss has not decreased for 3 consecutive validations, where the validation is conducted every 10 epochs. In the experiment of binding conformation generation, we only use the supervised dataset, thus we extend the training epochs for the autoencoder and the diffusion model to 500 and 1000, respectively. Consequently, the patience of learning rate decay is extended to 15 epochs for training the autoencoder. We keep other settings unchanged. The hyperparameters of PepGLAD used in our experiments are provided in Table 6.

Table 6. Hyperparameters of PepGLAD in sequence-structure codesign and binding conformation generation.

Name	Value		Description
	codesign	conformation	
Variational AutoEncoder			
embed size	128	128	Size of embeddings for residue types.
hidden size	128	128	Size of hidden layers.
h	8	-	Size of the latent variable for residue types in the sequences.
layers	3	3	Number of layers.
λ_1	0.1	0.0	The weight of KL divergence on the sequence.
λ_2	0.5	0.5	The weight of KL divergence on the structure.
λ_{CA}	1.0	1.0	The weight of C_α loss in \mathcal{L}_{aux} .
λ_{bond}	1.0	1.0	The weight of bond loss in \mathcal{L}_{aux} .
λ_{angle}	0.5	0.5	The weight of side-chain dihedral angle loss in \mathcal{L}_{aux} .
Latent Diffusion Model			
hidden size	128	128	Size of hidden layers in the denoising network.
layers	3	3	Number of layers.
steps	100	100	Number of diffusion steps.

G.2. Implementation of the Baselines

For **HSRN** (Jin et al., 2022), **dyMEAN** (Kong et al., 2023), and **DiffAb** (Luo et al., 2022), we directly integrate their official implementation into the same training framework as our PepGLAD, and adjust the batch size, learning rate, and training epochs to obtain the optimal performance. We outline the implementation of other baselines below:

RFDiffusion (Watson et al., 2023) We follow the official instruction to randomly select 20% of residues on the binding site as "hotspots", and generate the backbone via diffusion followed by cycles of inverse folding with ProteinMPNN (Dauparas et al., 2022) and full-atom structural refining with the officially provided Rosetta protocol.

AnchorExtension (Hosseinzadeh et al., 2021) It is implemented with the Rosetta suite, thus we resort to the official release of the pipeline protocols for docking and optimizing. We use the default parameters and generate 10 candidates for each

receptor due to its limitation of efficiency. We randomly pick one peptide in the training set with the same length as the reference peptide as the initial motif for docking.

FlexPepDock (London et al., 2011) We follow its official tutorial to implement this baseline in the C++ version of Rosetta.

AlphaFold2 (Jumper et al., 2021) We borrow the results from (Tsaban et al., 2022), which explores two strategy to use AlphaFold2 on peptide conformation generation, including modeling the receptor and the peptide as separate chains or link them together with long loops. The results contain a total of 10 candidates for each receptor, with 5 from the separate strategy and 5 from the linked strategy.